

AN EXPERIMENTAL INVESTIGATION
OF FATIGUE RELIABILITY LAWS

by

© YVES THERIAULT

A thesis submitted to the Faculty of Graduate
Studies and Research in partial fulfillment
of the requirements for the Degree of
Master of Engineering

Department of Mechanical Engineering
McGill University
Montreal, Quebec
Canada

February 1983

ABSTRACT

This thesis concerns the assessment of the validity of statistical functions that describe the scatter in fatigue data and the reliability of components subjected to fatigue loading situations. Attention is particularly focused on the "Provan law" which has been derived based upon a probabilistic description of the microstructural fatigue crack growth processes. The statistical laws are first succinctly described followed by the description and results of an experimental program specifically developed to ascertain their applicability, especially in relation to the "Provan law". This program consisted of performing strain controlled fatigue experiments on specially prepared oxygen-free-high-conductivity copper specimens. This was followed by a scanning electron microscope investigation of the fracture surfaces of a selected number of specimens in order to determine the basic material crack growth intensity parameter, λ , required for the implementation of the "Provan law". Secondly, the laws are compared both on the basis of computer generated curve fits of the fatigue data and on the results of the Komolgorov-Smirnov and Cramer-Von Mises statistical tests. In addition, a theoretical λ is evaluated and compared with its empirical (curve fit) and experimental counterparts. Finally, the applicability of the statistical functions in fatigue reliability is discussed.

RESUME

La présente thèse a pour objet l'évaluation de l'applicabilité de certaines fonctions statistiques à la représentation de la dispersion des résultats en fatigue et au calcul de la fiabilité de composantes mécaniques soumises à la fatigue. Une attention particulière est accordée à la "loi de Provan" qui a été récemment dérivée à partir d'un modèle probabiliste du processus de propagation d'une fissure en fatigue.

Les principales caractéristiques de chacune des fonctions sont premièrement présentées, suivies d'une description du programme expérimental qui a permis d'évaluer leur validité. Ce programme consistait, en premier lieu, à effectuer des tests de fatigue en contrôle de déformation sur des éprouvettes de cuivre pur spécialement préparées à cet effet. La seconde partie du programme fut d'observer au microscope électronique à balayage les surfaces de fracture d'un nombre choisi d'éprouvettes. Le but de ses observations était de déterminer, pour le matériau étudié, l'intensité de propagation d'une fissure de fatigue, λ , paramètre nécessaire à la vérification de la "loi de Provan".

Les fonctions sont ensuite comparées en se basant sur leur degré d'ajustement aux données expérimentales ainsi que sur les résultats des tests d'hypothèses de Komolgorov-Smirnov et de Cramer-Von Mises. De plus, une valeur théorique pour λ est calculée et comparée aux valeurs expérimentale et empirique obtenues à partir de l'analyse des résultats expérimentaux. Finalement, des conclusions sont tirées concernant l'utilisation des fonctions statistiques pour évaluer la fiabilité en fatigue.

ACKNOWLEDGEMENTS

The author is deeply indebted to Professor J.W. Provan, his research supervisor, whose guidance and encouragement were of tremendous help and whose dynamism was a constant source of motivation in the preparation and the completion of this thesis.

The author wishes to acknowledge the valuable advice provided by his colleague Louis Achard during the performance of the experiments.

A word of thanks is also given to Mrs. Evelyn Schliecker for the many hours of labour she spent in typing this thesis.

Finally, the financial assistance of the Mechanical Engineering Department of McGill University and of the Natural Sciences and Engineering Research Council is gratefully acknowledged.

TABLE OF CONTENTS

	<u>PAGE</u>
ABSTRACT	i
RESUME	ii
ACKNOWLEDGEMENTS	iii
TABLE OF CONTENTS	iv
LIST OF FIGURES	vii
LIST OF TABLES	ix
 CHAPTER 1 <u>INTRODUCTION</u>	 1
1.1 MOTIVATION	1
1.2 PREVIOUS STUDIES	3
1.3 THESIS DESCRIPTION	5
 CHAPTER 2 <u>REVIEW OF FATIGUE RELIABILITY THEORIES</u>	 7
2.1 THE EXPONENTIAL DISTRIBUTION	7
2.2 THE NORMAL DISTRIBUTION	8
2.3 THE LOG NORMAL DISTRIBUTION	10
2.4 THE GAMMA DISTRIBUTION	13
2.5 THE WEIBULL DISTRIBUTION	14
2.5.1 Two-Parameter Weibull	15
2.5.2 Three-Parameter Weibull	15
2.6 THE GUMBEL (EXTREME-VALUE) DISTRIBUTIONS	16
2.7 THE BIRNBAUM-SAUNDERS DISTRIBUTION	18
2.8 THE "PROVAN" DISTRIBUTION	21
2.9 SUMMARY	24
2.10 THESIS OBJECTIVES	25

	<u>PAGE</u>
CHAPTER 3 <u>EXPERIMENTAL INVESTIGATIONS</u>	26
3.1 MATERIAL	26
3.2 SPECIMEN DESIGN	26
3.3 SPECIMEN PREPARATION	26
3.3.1 Machining	27
3.3.2 Annealing	27
3.3.3 Polishing	27
3.3.4 Storage	28
3.4 TEST EQUIPMENT	28
3.4.1 The MTS Test Facility	28
3.4.1.1 Hydraulic Power Supply	29
3.4.1.2 Loading Unit	29
3.4.1.3 Control Console	31
3.4.2 The Scanning Electron Microscope	34
3.5 TESTING PROCEDURE	35
3.5.1 Fatigue Experiments	35
3.5.2 SEM Observations	36
CHAPTER 4 <u>ANALYSIS OF RESULTS</u>	38
4.1 DATA PRESENTATION	38
4.2 STATISTICAL INTERPRETATION OF DATA	38
4.2.1 Exponential	39
4.2.2 Normal	40
4.2.3 Log Normal	41
4.2.4 Gamma	41
4.2.5 Weibull (Two-parameter)	42
4.2.6 Gumbel (Largest and Smallest Values)	42
4.2.7 Birnbaum-Saunders	43
4.2.8 "Provan"	44
4.3 COMMENTS AND COMPARISONS	44
4.3.1 CDF Curves	44

	<u>PAGE</u>
4.3.1.1 Curve Fitting	44
4.3.1.2 Statistical Tests	45
4.3.2 The Fatigue Transition Intensity (λ)	47
CHAPTER 5 <u>CONCLUSIONS</u>	50
5.1 CONCLUDING REMARKS	50
5.2 PROPOSALS FOR FURTHER RESEARCH	51
REFERENCES	53
FIGURES	56
TABLES	75
APPENDIX A NUMERICALLY CONTROLLED MACHINING STEPS	87
APPENDIX B STEP-BY-STEP TESTING PROCEDURE FOR THE FATIGUE EXPERIMENTS	88
APPENDIX C COMPLEMENTARY INFORMATION	91
APPENDIX D DERIVATION OF THE "PROVAN" CDF	96
APPENDIX E CURVE FITTING PROGRAMS	99
APPENDIX F PLOTTING PROGRAM	103

LIST OF FIGURES

<u>FIGURE</u>		<u>PAGE</u>
2.1	Crack, interference model leading to the "Provan reliability law".	56
3.1	Fatigue specimen with tangentially blending fillets	57
3.2	Block diagram of the MTS test system	58
3.3	Hydraulic power unit of the MTS testing system	59
3.4	Loading unit of the MTS testing system	60
3.5	The MTS Axial extensometer	61
3.6	Control console of the MTS testing system	62
3.7	Scanning electron microscope	63
3.8	Schematic of the scanning electron microscope	64
3.9	Filtering circuit to detect specimen failure	65
4.1	Plot of the ranked experimental data	66
4.2	Exponential and normal CDF curve fits of the experimental fatigue data	67
4.3	Log normal and gamma CDF curve fits of the experimental data	68
4.4	Weibull and Gumbel (largest value) CDF curve fits of the experimental data	69
4.5	Gumbel (smallest value) and Birnbaum-Saunders CDF curve fits of the experimental data	70

<u>FIGURE</u>		<u>PAGE</u>
4.6	"Provan" CDF curve fit of the experimental data	71
4.7	Typical fractograph for OFHC copper. (Region at 2.9 mm from the initiation zone.)	72
4.8	Fractograph for OFHC copper. (Region at 1.7 mm from the initiation zone.)	73
4.9	Fractograph for OFHC copper. (Region near the final fracture zone.)	74

LIST OF TABLES

<u>TABLE</u>		<u>PAGE</u>
2.1	Main characteristics of the reliability laws	75
2.2a)	Exponential normal and log normal probability density functions	76
2.2b)	Gamma, Weibull and Gumbel probability density functions	77
2.2c)	Birnbaum-Saunders and "Provan" probability density functions	78
2.3	Reliability laws and their basic statistics	79
3.1	Specification and mechanical properties of OFHC brand copper	80
3.2	Statistics of the specimen test section measurements	81
4.1	Summary of the fatigue test conditions	82
4.2	Ranked fatigue data	83
4.3	Curve-fit root mean square errors	84
4.4	Results of the statistical tests	85
4.5	Theoretical, experimental and empirical values for the crack growth transition intensity parameter of the "Provan law"	86

CHAPTER 1

INTRODUCTION

1.1 MOTIVATION

It is nowadays recognized that the great majority of mechanical failures result from fatigue related degradation processes. In recent years, therefore, design engineers have shown an increasing concern about fatigue of materials in order to maintain an acceptable level of structural integrity for modern large structures and complex components subjected to more and more demanding service conditions. But, complexity and size become major obstacles when one has to perform real life tests to assess designs and design parameters. The required tests are either too costly or simply not feasible which forces the engineer to rely on data obtained by fatigue testing simple laboratory specimens. Besides, it is generally observed that these data exhibit a relatively large amount of scatter. This is true for constant as well as variable amplitude (and frequency) loading and for all materials.

The scatter in fatigue data has long been thought to be only attributable to the variations in test conditions. However, the test variables being severely controlled, there still remains an appreciable residual dispersion in the results that must consequently be associated with the material microstructure itself, that is, with the random distribution of lattice defects and impurity atoms on the submicroscopic scale, and with the variation in crystal size and orientation in the

material at the microscopic level. This attests to the random nature of fatigue and suggests a probabilistic rather than a deterministic approach to the problem. Thus, it is more appropriate to talk about the probability that a component will not fail instead of merely saying that it is not expected to fail. The evaluation of this probability of non-failure, more commonly known as reliability, becomes, then, one of the (if not the most important) critical design conditions, recalling that high reliability is synonymous of low overall costs. Therefore, there is an urgent need to provide the design engineer with ready-to-use probabilistic methods for — assessing the reliability of large structures and components.

Most of the fatigue reliability models that have been proposed and successfully used so far are more or less based on empiricism. That is, little or no effort has been made to describe the fatigue mechanisms in deriving these models. They usually require a substantial amount of test data to be confidently used which therefore restricts their application.

In recent years, new models that are based on a probabilistic description of the fatigue crack growth process have been developed. Of course, these models still require refinement and improvement before they emerge as "reliable" design tools, but they constitute a promising avenue of research that is certainly worthwhile exploring. It is the author's hope that the fruits of this advanced design philosophy will gain more and more acceptance in the engineering field.

1.2 PREVIOUS STUDIES

The study of scatter in fatigue data was placed on a sound footing by the work of Weibull [1] who, in 1949, presented a statistical function derived from a probabilistic characterization of the breaking strength of materials. Since then, the Weibull function has been frequently suggested as a time-to-failure model based on empirical grounds, and satisfactory representations have been obtained by Leiblein and Zelen [2], Kao [3] and Perry [4] in their studies on ball-bearings, electron tubes and transistors, respectively.

As fatigue became a more crucial problem in design, several other research engineers followed in Weibull's footsteps and proposed statistical models to describe the reliability of mechanical components, systems and structures that were constantly growing in size and complexity. Among the most familiar of these models are the exponential, normal, log normal, gamma, and Gumbel.

An acceptable justification for the assumption of an exponential distribution to life studies was initially discussed by Epstein [5] and by Davis [6]. Later, the exponential model was mathematically assessed as a failure law for complex equipment [7].

Few applications of the normal distribution as a reliability model are reported in the literature, the main reason being that, for a given set of fatigue data, one generally prefers to use more flexible (the normal distribution does not have a shape parameter) distributions, such as the gamma and Weibull, that adequately describe the scatter.

Until recently, the applicability of the log normal distribution has been limited to rare situations in small-particle statistics, economics and biology [8]. However, Howard and Dobson [9] and Peck [10] have extended its use to fracture problems. Its applicability as a failure distribution has been also indicated by the life-test sampling plans developed for it by Gupta [11].

Extensively used in the study of floods, aeronautics, geology and naval engineering [12] the Gumbel distribution can also be applied to life test and reliability situations where failure of components of systems are linked to extremal phenomena as discussed by Hahn and Shapiro [13] and also by Mann, Schafer and Singpurwalla [14].

In the past few years, more research effort has been devoted to the derivation of reliability models based on probabilistic interpretations of the fatigue process. Thus, Birnbaum and Saunders [15] have proposed a life distribution to characterize failures due to the extension of a fatigue crack. They have further used it, [16], to offer a probabilistic interpretation of Miner's rule. Birnbaum and Saunders have also found experimental support to their law from the work of Freudenthal and Shinozuka [17] who have presented a similar law substantiated by several sets of fatigue data. Subsequently, Payne [18] introduced a statistical reliability model for assessing the fatigue strength of aircraft structures. This model evaluates the random variability in crack propagation rates and the residual strengths of cracked structures at any stage of their life. More recently, Provan [19] has derived a reliability distribution based on probabilistic micromechanics concepts applied to the fatigue of polycrystalline metals. The theoretical

foundations of this microstructural interpretation of the scatter in fatigue data are given in [20] and have been experimentally assessed in [21].

1.3 THESIS DESCRIPTION

This thesis begins with a chapter reviewing the familiar empirical and semi-empirical laws used in fatigue reliability, namely, the exponential, normal, log normal, gamma, Weibull and Gumbel extreme value cumulative distribution functions. The not so familiar theoretical laws of Birnbaum-Saunders and Provan are also presented. A more comprehensive description of the "Provan law" is given since the assessment of its validity is the prime interest of the current investigation. The main characteristics of each distribution and their range of applications are discussed.

Chapter 3 is concerned with the experimental part of the thesis that consisted of two separate investigations: the fatigue experiments and the scanning electron microscope observations. A description of the specimen machining and preparation is first given. Then, the major components of the experimental equipment and also the experimental procedure are described.

The results of the experimental investigations are presented and analyzed in Chapter 4. Two methods of analysis, namely, the curve fitting and the statistical tests are applied to assess the adequacy of the above-mentioned reliability functions with respect to the collected fatigue data. The additional method for verifying the validity of the "Provan law" through the results of the microscope observations is also explained.

The final chapter presents the conclusions and proposals for further research.

In order to lighten the text, complementary information such as definitions, computer programs, and detailed procedures are given in the appendices.

CHAPTER 2

REVIEW OF FATIGUE RELIABILITY THEORIES

The number of continuous distributions available which empirically describe the scatter in fatigue data is considerable. This chapter deals both with the most common and two recently derived theoretical functions pertaining to fatigue reliability. In describing the distributions, the emphasis is put on the principal characteristics and on the domain of applicability.

2.1 THE EXPONENTIAL DISTRIBUTION

The exponential probability density function (p.d.f.) is undoubtedly the most commonly used time-to-failure distribution. It is as important in reliability as the normal distribution is in other fields of statistics. Unfortunately, in many cases, the choice of the exponential distribution as a failure model is based on the fact that it is easy to apply rather than on the understanding of the physical problem.

The p.d.f. for an exponentially distributed random variable x is given by:

$$f(x;\delta) = \frac{1}{\delta} e^{-x/\delta} : x \geq 0 ; \delta > 0 \quad (2.1)$$

where the parameter $1/\delta$ is referred to as the hazard rate (see Appendix C). This parameter being constant, the exponential model is characterized (and, in a certain way, limited) by the property known as complete "lack of memory".

Thus, assuming an exponentially distributed time-to-failure, the probability of failure of a given unit during a specific time interval depends only on the length of the interval and is therefore the same irrespective of whether the unit has previously survived 100 hours or 1000 hours.

The exponential distribution has been found more appropriate as a reliability model for complex systems or assemblies. However, it is also applicable for components in cases where replacement is carried out during the in-usage portion of the component life, that is, before wear out occurs.

The cumulative distribution function can be obtained from the p.d.f. through the familiar relation:

$$\text{CDF} = F(x) = \int_{-\infty}^x \text{p.d.f. } dx, \quad (2.2)$$

which yields a rather simple expression for an exponential variable, namely;

$$F(x) = 1 - e^{-x/\delta}, \quad (2.3)$$

Finally, it should be mentioned that the exponential distribution is a special case of both the Weibull and the gamma distributions that are further discussed in this chapter.

2.2 THE NORMAL DISTRIBUTION

The normal or Gaussian distribution is the best known and most frequently used statistical model. It owes its popularity principally to

the fact that it conforms approximately to the observed distribution of many physical quantities. It was first introduced in 1733 through the work of De Moivre who derived it as a limiting case of the binomial distribution. The normal distribution was also known to Laplace no later than 1774, however, through historical mistake, its discovery has been attributed to Gauss whose first published reference to it appeared in 1809.

A random variable is said to be normally distributed if its p.d.f. has the form:

$$f(x) = \frac{1}{\sqrt{2\pi} \sigma} \exp\left[-\frac{1}{2} \left(\frac{x-\mu}{\sigma}\right)^2\right] ; \quad (2.4)$$

$$-\infty < x < \infty ; -\infty < \mu < \infty ; \sigma > 0 .$$

This simple shape distribution is symmetric about its mean μ and its degree of dispersion is represented by the parameter σ that is also known as the standard deviation.

The associated CDF to (2.4) is given by:

$$F(x) = \frac{1}{\sigma\sqrt{2\pi}} \int_{-\infty}^x \exp\left[-\frac{1}{2} \left(\frac{\xi-\mu}{\sigma}\right)^2\right] d\xi , \quad (2.5)$$

whose evaluation is far from straightforward. But, by simply making the change of variable $z = (x-\mu)/\sigma$, (2.5) becomes:

$$F(z) = \frac{1}{\sqrt{2\pi}} \int_{-\infty}^z \exp\left(-\frac{s^2}{2}\right) ds , \quad \text{with } s = \frac{\xi-\mu}{\sigma} , \quad (2.5a)$$

a simpler function that is tabulated in any fundamental book on statistics.

The random variable z is called the standard normal variate and follows a normal distribution with $\mu = 0$ and $\sigma = 1$ [14].

The validity of the normal distribution as a time-to-failure model is questionable since the normal variate x includes negative values. However, when $\mu \geq 3\sigma$, the basic requirements for any life model to be acceptable, namely,

$$\int_0^{\infty} f(x) dx = 1 \quad (2.6)$$

is satisfactorily met (error ~0.14%). For the other cases, the distribution is truncated to:

$$\bar{F}(x) = \frac{1}{\kappa \sigma \sqrt{2\pi}} \exp\left[-\frac{1}{2} \left(\frac{x-\mu}{\sigma}\right)^2\right] ; \quad (2.7)$$

$$0 < x < \infty ,$$

where κ is the normalizing constant such that:

$$\int_0^{\infty} \bar{F}(x) dx = 1 \quad (2.6a)$$

2.3 THE LOG NORMAL DISTRIBUTION

A random variate x is said to be log normally distributed if its logarithm follows a normal distribution with parameters μ' and σ' . The p.d.f.

of x is then given by:

$$f(x) = \frac{1}{\sigma' x \sqrt{2\pi}} \exp \left[-\frac{1}{2} \left(\frac{\ln x - \mu'}{\sigma'} \right)^2 \right] \quad (2.8)$$

$$0 < x < \infty ; 0 < \mu' < \infty ; \sigma' > 0 ,$$

and its CDF by:

$$F(x) = \frac{1}{\sigma' \sqrt{2\pi}} \int_0^x \frac{1}{\xi} \exp \left[-\frac{1}{2} \left(\frac{\ln \xi - \mu'}{\sigma'} \right)^2 \right] d\xi , \quad (2.9)$$

The log normal distribution has various shapes and is characterized by a right skewness as shown in Table 2.1a). Note that μ' and σ' represent here the scale and shape parameters, respectively, and not the location and scale parameters as for the normal distribution.

Setting $y = \ln x$ in (2.9) we obtain:

$$F(y) = \frac{1}{\sigma' \sqrt{2\pi}} \int_{-\infty}^y \exp \left[-\frac{1}{2} \left(\frac{\alpha - \mu'}{\sigma'} \right)^2 \right] d\alpha , \quad (2.10)$$

which is very similar to (2.5) and can therefore be evaluated using the same tables after putting it into the form of (2.5a).

The fundamental derivation of the logarithmic normal distribution is carried out by considering a physical process wherein failure is due to the growth of a fatigue crack. For this reason, the utilization of this distribution for fatigue failure problems seems fully justified.

Let $X_1 < X_2 < \dots < X_n$ be a sequence of random variables denoting the size of a fatigue crack at different stages of its growth. If we assume a proportional effect, [22], for the growth of these cracks, it follows that the crack growth at stage i , $X_i - X_{i-1}$, is randomly proportional to the size of the crack, X_{i-1} , and the component fails when the crack length reaches X_n .

Let $X_i - X_{i-1} = \pi_i X_{i-1}$, $i = 1, 2, \dots, n$, where π_i is a constant of proportionality varying in a random manner with i . The initial crack size X_0 is interpreted as the size of minute flaws, voids and the like in the components. Finally, the π_i are assumed to be independently distributed random variables having not necessarily the same distribution for all i 's.

Hence:

$$\frac{X_i - X_{i-1}}{X_{i-1}} = \pi_i \quad ; \quad i = 1, 2, \dots, n \quad , \quad (2.11)$$

or:

$$\sum_{i=1}^n \pi_i = \sum_{i=1}^n \frac{\Delta X_{i-1}}{X_{i-1}} \quad , \quad (2.12)$$

where $\Delta X_{i-1} = X_i - X_{i-1}$. For the limit case, namely, $\Delta X_{i-1} \rightarrow 0$ and n becomes large, we get:

$$\sum_{i=1}^n \pi_i = \int_{X_0}^{X_n} \frac{1}{X} dX = \log X_n - \log X_0 \quad , \quad (2.13)$$

or

$$\log X_n = \sum_{i=1}^n \pi_i + \log X_0 \quad . \quad (2.14)$$

Since the π_i , by assumption, are independently distributed variates, by the central limit theorem (see Appendix C), they converge to a normal distribution. Therefore, $\log X_n$ is asymptotically normally distributed and hence X_n has a logarithmic normal distribution.

2.4 THE GAMMA DISTRIBUTION

The gamma distribution is a natural extension of the exponential distribution, being the appropriate model for the time required for a total of exactly n independent events to take place if events occur at a constant rate α , i.e., each event is exponentially distributed. In reliability terms, this means that a system or assembly time to failure is gamma distributed if the system failure occurs as soon as exactly n subfailures have taken place and if subfailures occur independently at a constant rate α .

The gamma p.d.f. is:

$$f(x) = \alpha^n \frac{x^{n-1}}{\Gamma(n)} e^{-\alpha x} ; x > 0, \alpha, n > 0 \quad , \quad (2.15)$$

where $\Gamma(n)$ is the well-known gamma function, namely:

$$\Gamma(n) = \int_0^{\infty} x^{n-1} e^{-x} dx \quad , \quad (2.16)$$

and n and α are the shape and scale parameters respectively.

The wide variety of gamma distribution shapes certainly accounts for the frequent use of this model, especially in reliability. Thus, many phenomena that cannot be justified theoretically as gamma variates, have,

nevertheless, been found empirically to be well approximated by the gamma p.d.f.

The gamma CDF is written as:

$$F(x) = \frac{\alpha^\eta}{\Gamma(\eta)} \int_0^x t^{\eta-1} e^{-\alpha t} dt, \quad (2.17)$$

which is also known as the incomplete gamma function and can be evaluated through the tables of the function $I(u, p)$ [23] where u and p are defined as follows:

$$u = \frac{\alpha x}{\sqrt{\eta}} \quad \text{and,} \quad p = \eta - 1. \quad (2.18)$$

2.5 THE WEIBULL DISTRIBUTION

In 1949, a Swedish research engineer named Waloddi Weibull proposed a probability density function [1] for the interpretation of fatigue data. Since then, however, the application of this failure distribution has been extended to many other engineering problems. The great versatility of the Weibull distribution stems from the possibility to adjust it to fit the many cases where the hazard rate either increases or decreases. The Weibull distribution is also known to statisticians as the Fisher-Tippett Type III asymptotic distribution of the smallest extreme, that is to say that it can also be derived from the extreme-value theory [14].

2.5.1 Two-Parameter Weibull

For certain statistical phenomena, one can reasonably assume that the lower bound of the associated random variable is equal to zero. For those cases, the Weibull p.d.f. is written as:

$$f(x) = \frac{\beta x^{\beta-1}}{\theta^{\beta}} \exp\left[-\left(\frac{x}{\theta}\right)^{\beta}\right] ; \quad (2.19)$$

$$\beta, \theta > 0 ; x \geq 0 ,$$

and the CDF as:

$$F(x) = 1 - \exp\left[-\left(\frac{x}{\theta}\right)^{\beta}\right] , \quad (2.20)$$

where, θ is the characteristic value corresponding to the $(e-1)/e$ or 63% probability point, and is known as the scale parameter, and β is the shape parameter.

2.5.2 Three-Parameter Weibull

The more general form of the Weibull distribution takes into account an arbitrary origin for the random variable by introducing a location parameter, say θ_0 . This is needed, for instance, in life testing when components are designed to last "at least" a certain time. The p.d.f. and CDF then respectively become:

$$f(x) = \beta \frac{(x-\theta_0)^{\beta-1}}{(\theta-\theta_0)^{\beta}} \exp\left[-\left(\frac{x-\theta_0}{\theta-\theta_0}\right)^{\beta}\right] , \quad (2.21)$$

and:

$$F(x) = 1 - \exp\left[-\left(\frac{x - \theta_0}{\theta - \theta_0}\right)^\beta\right], \quad (2.22)$$

with $\theta_0 \geq 0$.

2.6 THE GUMBEL (EXTREME-VALUE) DISTRIBUTIONS

Failure of components or systems may frequently be related to causes that depend directly on either the smallest or the largest value in a particular sample distribution. For example, in fatigue tests at a constant stress, failure may be dependent on the strength of the weakest of many "elements" in a given material, or it may be dependent on the size of the largest flaw. In those cases we are interested in the distribution of the smallest value (minimum element strength) or the largest value (maximum flaw size) in a sample from some (generally unknown) initial distribution. The smallest or largest element distribution will, in general, be a function of the sample size, n , and on the nature of the initial distribution. However, if n becomes large and if the initial distribution is of the "exponential type" (such as exponential, normal, and log-normal distributions) Cramer has shown [24] that the cumulative distribution of the smallest (or largest) value converges asymptotically towards the so-called Type I extreme value for the smallest (or largest) extreme distribution. Because this distribution was extensively used by Gumbel [25] in his study of extremal phenomena, it is also known as the Gumbel distribution. Thus, if the initial distribution is of such a form that it tends to zero exponentially as the associated random variable tends to $-\infty$, the limiting cumulative distribution is referred to as

the Gumbel distribution for the smallest extreme and is written as:

$$F(x) = 1 - \exp[-\exp(\frac{x-\alpha}{\delta})] ; \quad (2.23)$$

$$-\infty < x < \infty ; \delta > 0 ; -\infty < \alpha < \infty ,$$

and its related p.d.f. as:

$$f(x) = \frac{1}{\delta} \exp[\frac{1}{\delta} (x-\alpha) - \exp(\frac{x-\alpha}{\delta})] \quad (2.24)$$

Similarly, if the initial distribution tends to zero exponentially as the random variable tends to $+\infty$, we obtain the Gumbel distribution for the largest extreme, given by:

$$F(x) = \exp\{-\exp[-(\frac{x-\alpha}{\delta})]\} \quad (2.25)$$

and the p.d.f. by:

$$f(x) = \frac{1}{\delta} [-\frac{1}{\delta} (x-\alpha) - \exp(-\frac{x-\alpha}{\delta})] \quad (2.26)$$

The two Gumbel density functions, that is, Equations (2.24) and (2.26) are mirror images of each other as depicted in Table 2.2c. One should also note that although the preceding results are asymptotic (i.e., they are derived from $n \rightarrow \infty$) the extent to which they are applicable for moderate size n , or in other words the rate of convergence, depends on the initial distribution. For example, fewer observations are required for the distribution of the largest value to approach the Gumbel distribution if the initial distribution is exponential than if it is normal.

2.7 THE BIRNBAUM-SAUNDERS DISTRIBUTION

The Birnbaum and Saunders fatigue-life model, proposed in 1979 [15], assumes that fatigue failure is due to the growth and ultimate extension of a crack past a critical length. At each oscillation of the imposed load, this crack is extended by a random amount, the randomness being the result of variation in the material, the magnitude of the stress, the specimen geometry and other such factors. The extension of the fatigue crack is then represented by a nonnegative random variable whose two-parameter cumulative distribution function, namely, the Birnbaum-Saunders distribution, will now be derived.

In their approach, Birnbaum and Saunders first consider a specimen that is subjected to identical sequences (i.e., cycles) of m loads, $\{l_i\}$ $i = 1, 2, \dots, m$, each load causing a deformation of the specimen, thereby imposing a stress on it. The loading scheme can be seen as follows:

$$\begin{array}{ll} l_1, l_2, \dots, l_m & \text{cycle 1} \\ l_{m+1}, l_{m+2}, \dots, l_{2m} & \text{cycle 2} \\ \vdots & \\ l_{jm+1}, l_{jm+2}, \dots, l_{jm+m} & \text{cycle (j+1)} \end{array}$$

with $l_{jm+i} = l_{km+i}$ for all $j \neq k$. Then, it is assumed that the loading is continuous which implies that for all $i = 1, 2, \dots, m$

$$l_{i+1}(0) = l_i(1) = l_{i-1}(0) \quad .$$

Having established the physical framework, two fundamental assumptions are next made. The first one is that the incremental extension X_i due to the load l_i in the cycle j is a random variable whose distribution

is governed by all the loads ℓ_j , $j < i$, and the actual crack extensions that have preceded it in cycle j alone. The second assumption concerns the total crack extension Y_j due to the j^{th} cycle that is taken as a random variable with mean μ and variance σ^2 , for $j = 1, 2, \dots$. Thus, we have

$$Y_{j+1} = X_{jm+1} + X_{jm+2} + \dots + X_{jm+m}$$

for cycle $(j+1)$ and under a repeated application of n cycles, the total extension of a crack in a specimen is written as:

$$W_n = \sum_{j=1}^n Y_j \quad (2.27)$$

The first assumption is rather restrictive in the sense that it ensures that the total random crack extensions, Y_j 's, are independent from cycle to cycle. This hypothesis is certainly not valid for several applications although Birnbaum and Saunders have found it plausible in many aeronautical fatigue studies [15].

Finally, defining C as the integer random variable that denotes the number of cycles at which W_n exceeds a critical value, ω , the Birnbaum-Saunders fatigue failure law is expressed as:

$$P(C \leq n) = P(W_n \geq \omega) = 1 - P\left(\sum_{j=1}^n Y_j \leq \omega\right) \quad (2.28)$$

But, from the second assumption we know that the $Y_{j,s}$ have a mean μ and a variance σ^2 ; thus, the $Y_{j,s}$ can be standardized to yield:

$$P(C \leq n) = 1 - P\left(\sum_{j=1}^n \frac{Y_{j,s} - \mu}{\sigma\sqrt{n}} \leq \frac{\omega - n\mu}{\sigma\sqrt{n}}\right) \quad (2.29)$$

Next, from the assumption on the independence of the $Y_{j,s}$ and using the central limit theorem and the symmetry of the normal distribution, (2.29) can be rewritten as

$$\begin{aligned} P(C \leq n) &= 1 - \Phi\left(\frac{\omega - n\mu}{\sigma\sqrt{n}}\right), \\ &= \Phi\left(\frac{n\mu}{\sigma\sqrt{n}} - \frac{\omega}{\sigma\sqrt{n}}\right), \end{aligned} \quad (2.30)$$

where

$$\Phi(x) = \int_{-\infty}^x \frac{1}{\sqrt{2\pi}} e^{-s^2/2} ds \quad (2.31)$$

Finally, defining

$$\alpha = \frac{\sigma}{\sqrt{\mu\omega}} \quad \text{and} \quad \beta = \frac{\omega}{\mu},$$

the recognizable form of the Birnbaum-Saunders law is obtained, namely

$$F_N(n; \alpha, \beta) = \Phi\left\{\frac{1}{\alpha} \left[\left(\frac{n}{\beta}\right)^{1/2} - \left(\frac{n}{\beta}\right)^{-1/2}\right]\right\} \quad (2.32)$$

The parameters α and β can be interpreted as shape and scale, respectively.

Now, from the above derivation it follows that:

$$Z = \frac{1}{\alpha} \left[\left(\frac{N}{\beta} \right)^{1/2} - \left(\frac{\beta}{N} \right)^{1/2} \right], \quad (2.33)$$

is distributed normally with mean 0 and variant 1 and hence the probability density function associated with (2.32) is inferred as:

$$f_N(n; \alpha, \beta) = \frac{1}{2\sqrt{2\pi} \alpha^2 \beta n^2} \frac{(n^2 - \beta^2)}{(n/\beta)^{1/2} - (\beta/n)^{1/2}} \\ \times \exp \left[-\frac{1}{2\alpha^2} \left(\frac{n}{\beta} + \frac{\beta}{n} - 2 \right) \right] \quad (2.34)$$

2.8 THE "PROVAN" DISTRIBUTION

The "Provan" fatigue reliability function results from a probabilistic micromechanics approach to the description of fatigue failure of polycrystalline metals [20]. Based on this approach, a statistical model describing the fatigue crack initiation process was first developed to evaluate the number of cycles, N_0 , required to initiate a crack. Subsequently, a linear pure birth Markov stochastic process was used as a model to describe the scatter in the number of cycles involved in the propagation stage. In this analysis, the crack front is characterized at each cycle i by the Gaussian pair $(\mu_a; V_a)$ which are the mean and the variance of the crack length, respectively. Specifically, this pair is expressed as shown in [20] by:

$$(\mu_a; V_a) = (\mu_{a_0} e^{\lambda i}; \mu_{a_0} \Delta x_1 e^{\lambda i} (e^{\lambda i} - 1)) ; \quad (2.35)$$

$$0 \leq i \leq N_p ,$$

where,

$\lambda = \frac{\phi \mu_{a_0}}{N_0 \Delta x_1}$ is the crack growth intensity
 μ_{a_0} is the mean of the initiated crack length, and
 Δx_1 is the experimental accuracy of the crack measuring technique (see Section 4.3.2).

The constant ϕ in the above expression for λ is a material parameter numerically determined from experimental results by means of an iterative computer program described in [26]. Once this parameter is known, one can infer the crack growth characteristics given by (2.35) for any cycle i .

An experimental program detailed in [21] was conducted in order to check on the validity of expression (2.35). This study, involving fatigue experiments as well as microscopic observations of the fracture surfaces, showed satisfactory agreement as far as the mean, μ_a , is concerned but clearly indicated that the expressions for the variance in (2.35ii) yielded an overestimate of the scatter in crack growth. From the results of the same study, it was also observed that the variance of the crack length distribution tends to a stabilized value, V_{ac} , near the final fracture zone. This suggests the change of (2.35) into:

$$(\mu_a; V_a) = (\mu_{a_0} e^{\lambda i}; V_{ac}) ; 0 \leq i \leq N_p . \quad (2.36)$$

The above relation was chosen for the derivation of the micro-mechanic reliability law since the latter is rather related to what happens to the crack near the final fracture than to what occurs at the initiation zone. The progression of the crack length density function represented by (2.36) is illustrated in Fig. 2.1. Here, the density function is assumed to be Gaussian to simplify the mathematical manipulations. However, this is not a limitation since any other distribution defined by the basic variables $(\mu_a; V_a)$ could in theory be used.

As shown in Fig. 2.1, the crack length distribution translates until it interferes with the critical crack length distribution represented by the pair $(\mu_{af}; V_{af})$ which is a material characteristic. The latter distribution is taken as a delta function at μ_{af} , again for simplification purposes. The amount of $(\mu_a; V_a)$ overlapping μ_{af} as i increases is essentially the basis of the "Provan reliability law". This amount can be written as:

$$Q_i = \int_{\mu_{af}}^{\infty} p_a(i) da = \frac{1}{\sqrt{2\pi}} \int_{Z_i}^{\infty} \exp\left[-\frac{s_i^2}{2}\right] ds_i, \quad (2.37)$$

where

$$s_i = \frac{a - \mu_{ai}}{\sqrt{V_{ac}}}, \quad (2.38)$$

and

$$Z_i = \frac{\mu_{af} - \mu_{ai}}{\sqrt{V_{ac}}}, \quad (2.39)$$

is the failure coupling coefficient which itself is normally distributed with

mean 0 and variance 1 [14]. But, since $Z_i = (\mu_{af} - \mu_{ai}) / \sqrt{V_{ac}}$ is a known function of i , and knowing that a_i is Gaussian distributed with parameters given by (2.36), it follows from the fundamental relationship [27]:

$$p_{N_p} = p_{Z_i}(Z_i) \left| \frac{dZ_i}{di} \right|, \quad (2.40)$$

that the reliability density function, in terms of i , becomes:

$$p_{N_p}(i) = \frac{\mu_{a_0} \lambda}{\sqrt{2\pi V_{ac}}} \exp \left\{ \lambda i - \frac{(\mu_{a_0} \exp[\lambda i] - \mu_{af})^2}{2V_{ac}} \right\}. \quad (2.41)$$

The associated cumulative form to (2.41) is then derived as:

$$P_{N_p}(j) = \int_{-\infty}^j p_{N_p}(i) di = \frac{1}{2} \left\{ \operatorname{erf} \left(\frac{\mu_{a_0} e^{\lambda i} - \mu_{af}}{\sqrt{2V_{ac}}} \right) + \operatorname{erf} \left(\frac{\mu_{af}}{\sqrt{2V_{ac}}} \right) \right\}, \quad (2.42)$$

and hence the "Provan reliability law" is simply expressed as $R_j = 1 - P_{N_p}(j)$ which is a monotonically decreasing function of j . The detailed derivation of (2.42) is given in Appendix D.

2.9 SUMMARY

A few brief comments and a listing of each of the statistical models discussed in this chapter are given in Tables 2.1 a) and b). Plots of the probability density functions associated with these models are shown in Tables 2.2 a) through c). These plots are to illustrate the influence of the different parameters on the distribution shape. Finally, the cumulative distribution functions introduced in the previous sections are summarized in

Tables 2.3 a) and b). In the latter tables, erfc stands for the complementary error function which is defined as

$$\text{erfc}(x) = \frac{2}{\sqrt{\pi}} \int_x^{\infty} e^{-t^2} dt$$

and Γ is the incomplete gamma function tabulated in [23].

2.10 THESIS OBJECTIVES

The main objective of the present work is, then, to assess the validity of the reliability laws presented in this chapter by means of the experimental program further described in Chapter 3. Special attention is given to the "Provan law" that, *if experimentally substantiated*, will enable the design engineer to estimate the reliability of large structures or components based upon stochastic and probabilistic interpretations of the microstructural fatigue degradation processes. This, in fact, constitutes the long term aim of the research program of which this thesis is only a stage.

CHAPTER 3

EXPERIMENTAL INVESTIGATIONS

3.1 MATERIAL

The prime concern for selecting the material was obviously to find a metal whose fatigue fracture surface exhibits distinct striation profiles. This important feature has been observed in a previous experimental study [21] carried out on oxygen-free-high-conductivity (OFHC) brand copper. Therefore, this material was again chosen for the fatigue experiments reported in this chapter.

Specifications and some average properties of OFHC copper prior to test specimen preparation are presented in Table 3.1. For more information the reader is referred to [28].

3.2 SPECIMEN DESIGN

The design of the specimens was carried out as per the requirements of the ASTM E466 standard [29]. Based on those requirements and also on the form of available metal stock, the specimen dimensions given in Fig. 3.1 were calculated. A circular configuration was chosen for the specimen cross sections to minimize the machining time.

3.3 SPECIMEN PREPARATION

The specimen preparation is recognized to be the most crucial part of a fatigue test program since it strongly influences the resulting fatigue data, especially when a statistical study is performed. Therefore, the fatigue test specimens were prepared with great care and utmost precision following the general procedure outlined in the ASTM E466 standard. In this section the

main stages in the specimen preparation are succinctly described in chronological order.

3.3.1 Machining

The specimens were first cut into 13 x 1.6 x 1.6 cm square bars from a 40.2 x 30.5 x 1.6 cm OFHC copper plate supplied by Amax Inc., New Jersey. These bars were then made circular (1.3 cm dia.) by turning them on a lathe. Next, the ends of the specimens were faced to bring down their length to 12.7 cm. Finally, the blending fillet radii and the test section were machined on a numerically controlled (N/C) lathe to the dimensions shown in Fig. 3.1. The program used for this last machining step is given in Appendix A.

3.3.2 Annealing

Annealing of the specimen was necessary in order to avoid any deleterious effect of the residual stresses introduced during the machining process. The specimens were put into a Lindberg Hevi-Duty furnace with some charcoal to prevent them from oxydizing. They were then progressively heated to 500°C, held at this temperature for half an hour and free-cooled to the ambient temperature.

3.3.3 Polishing

Since the great majority of fatigue failures originate at the surface, too much emphasis cannot be placed on the importance of surface finish. Any incrustated dirt, flaws or geometrical discontinuities must, therefore, be eliminated to minimize the possibility of premature crack initiation.

In our case, the specimens were covered by a thin layer of carbon as a result of the annealing process. This layer as well as the scratches caused by machining were removed by hand-polishing with successively finer grade abrasive papers, namely, 200, 400 and 600 grit standard silicone carbide papers. Polishing was always performed in the specimen's longitudinal direction and visual inspections at 20x were conducted on all specimens to ensure that, at this magnification, no cracks or machining marks approximately perpendicular to the length of the specimens were present.

After polishing, the test section of the specimens was measured at four different locations by means of a Nikon V-16 profile projector. The statistics of these measurements are presented in Table 3.2.

3.3.4 Storage

Prior to storage the specimens were cleaned with acetone using a soft piece of cloth and they were afterwards numbered at one end with metal punches. Specimens were then stored in airtight transparent plastic containers with some dessicant (BDH-Drierite-8 mesh) to prevent moisture from altering their surface before the actual fatigue tests.

3.4 TEST EQUIPMENT

3.4.1 The MTS Test Facility

The fatigue tests were performed on a MTS closed-loop electrohydraulic testing system. A block diagram of the MTS system is shown in Fig. 3.2. The major units of the system, namely, the hydraulic power supply, the loading and the control units are briefly described in the next subsections. A more comprehensive description may be obtained from [21,30].

3.4.1.1 Hydraulic Power Supply

The hydraulic power supply (HPS), illustrated in Fig. 3.3, uses a 37.3 kW (50 HP) motor to drive a fixed-volume (76 l/min) pump that provides the hydraulic power to the loading unit. The output pressure of the pump can be either low (0.2 MPa) or high and adjustable up to a continuous pressure of 20 MPa depending on the selection made on the remote control panel (see sections 3.4.1.3).

The HPS incorporates a fluid-to-water heat exchanger to maintain the working fluid temperature below a maximum safe value that corresponds to an optimum system performance. If the fluid temperature exceeds a preset limit, a temperature-sensitive switch will open and turn the HPS off.

3.4.1.2 Loading Unit

The loading unit, shown in Fig. 3.4, is mainly composed of the load frame, the hydraulic actuator, the servovalves, the transducers, and the grips.

Supporting the loading components is the load frame which is rated at ± 100 kN in static loading. This structure consists of two vertical columns that join a movable crosshead and a fixed platen. The crosshead may be raised or lowered by means of hydraulic lifts to accommodate specimens of various lengths. Once in position, the crosshead is hydraulically locked to prevent slippage or backlash.

The axial load function is applied to test specimens through a hydraulic linear actuator. The piston of this actuator has a 15 cm stroke and a 47.3 cm² effective area which, times the maximum available pressure (i.e., 20 MPa), gives a limit static load capacity of ± 100 kN.

The servovalve is an electro-mechanical device that controls the actuator movement. It converts the control signal from the servocontroller (see next sub-section) to a mechanical movement of an internal spool. This allows the high-pressure fluid to flow into the cylinder and to act on either side of the piston, depending on the polarity of the control signal. On the present test rig, two servovalves are mounted in parallel, using a dual manifold, to double the flow rating and to increase the system response.

The load applied on the specimens was monitored by means of a resistive bridge load cell having a static and a dynamic loading capacity of respectively ± 100 kN and ± 75 kN. This transducer provides an output voltage directly proportional to applied force. The load cell calibration was checked using a Morchouse Proving Ring #843 (91 kN capacity). The deviation from linearity was found to be within acceptable limits for the load range used in the experiments (i.e., ± 20 kN).

Mounted on the hydraulic actuator is a linear variable differential transformer (LVDT) that generates an A-C output voltage in direct proportion to displacement of the actuator piston.

The gage section strain of the specimens was measured through a uniaxial extensometer shown in Fig. 3.5. This contacting type sensor is again of the resistive bridge category and is characterized by good stability and reliability. The linearity of the extensometer output was checked by means of a micrometer having a $2.54 \mu\text{m}$ accuracy. The absolute percent error was found to be less than 2% for the four strain ranges of the D-C conditioner (see next sub-section).

For our fatigue tests, a pair of self-aligning grips was used to clamp the specimens in the load train. Both grips are hydraulically actuated to provide a constant specimen gripping force independent of test load. But, the most interesting particularity of the grip design is its hydraulically locked spherical seat arrangement that allows the grip head to compensate for up to 0.01 radians (0.5 degrees) angular specimen misalignment. Bending due to a poorly machined specimen, misaligned test fixtures or other causes can thus be minimized by the swivelling action of the spherical seats.

3.4.1.3 Control Console

This unit precisely controls the test program and performs the readout of test data. The various modules incorporated in the control unit are presented in Fig. 3.6. The function and important features of these modules are summarized below.

The master control panel centralizes the electrical power distribution to all system components, thus eliminating the need to turn each of them on and off individually. An interlock built-in circuit automatically removes hydraulic power if any abnormal condition, such as fluid over-temperature or low levels in the HPS reservoir, occurs.

The controller constitutes the "brain module" of the MTS system. It performs the closed loop control functions and contributes to the system programming, failsafe, and readout functions through plug-in sub-modules. These are the feedback selector, the servocontroller, the valve driver, the limit detector, and the A-C and two D-C transducer conditioners.

While a mechanical input is applied on the specimen by the hydraulic actuator, the transducer conditioners supply the excitation voltage to their respective transducer (A-C for the LVDT and D-C for the load cell and the extensometer) and conditions the output voltages to be fed into the feedback selector. The latter selects the output of a particular transducer as a feedback signal that is processed by the servocontroller (the selected input is then called the controlled variable). Next, the servocontroller compares the feedback and the command signals and generates a correction or control signal that operates the servovalves after having been amplified by the valve driver sub-module. The command signal is a combination of a static signal generated by the controller and a dynamic programming signal supplied by the function generator.

Although, for our fatigue tests, only a sine function was used as part of the command signal, the digital function generator output is not limited to this particular waveform. It can actually generate other cyclic functions such as haversine and haversquare, with frequency variation from .00001 to 990 Hz, or programmable and adjustable ramp functions such as ramp, dual slope, triangle, saw tooth, and trapezoid. The ramp functions are adjustable from 0.001 to 990,000 seconds. All these waveforms start from zero and may be positive or negative going when started.

The fatigue test cycles were monitored by means of an electro-mechanical counter. This module is provided with three registers: the preset count register that enables the operator to set a desired number of cycles, the actual count register that reads the number of cycles already applied to the specimen for a given test run, and the total count register

that accumulates counts from test run to test run. When the actual count reaches the preset count the test run is automatically stopped (i.e., the programmer and the HPS are shut off). If the test is interrupted due to specimen failure, electrical power failure, or any action of the operator, the number of cycles to stop will be retained in the registers.

Another component that adds to the possibilities as well as to the safety of the MTS system is the limit detector. This sub-module monitors the three test variables (i.e., load, strain and stroke) simultaneously and, when any of these variables exceeds preset limits, initiates one of the following outputs:

- An upper or lower limit indicator (on the controller front panel) lights.
- Same as above plus an interlock opens, stopping the test and shutting off the HPS.
- The function generator output level changes to a preprogrammed level.

Throughout the experiments, test data could be visualized on a microprocessor-based data display. At the onset of each test, the strain applied on the specimen (i.e., the controlled variable) was adjusted from the readout of this module. Data were either displayed in volts or in pre-defined engineering units (load in pounds, strain in percent and stroke in inches) that had been previously stored in the random access memory (RAM) of the module.

As a complementary piece of equipment, a X-Y plotter was used to draw the load versus strain curves (hysteresis loops) periodically during the fatigue experiments.

3.4.2 The Scanning Electron Microscope

The second part of the experimental work was to observe the micro-morphology of the specimen fracture surfaces in order to determine an experimental value for the crack growth intensity, λ , previously discussed in Section 2.8. These microscopic observations were performed by means of a scanning electron microscope (SEM) whose photograph is shown in Fig. 3.7.

The SEM is one of the most versatile instruments available for the examination and analysis of the microstructural characteristic of solid objects. The most appreciated features of the SEM are a high resolution, a large depth of focus which results in a three dimensional appearance of the SEM images, and a capability to observe specimens at very low magnification.

The major SEM components are schematically represented in Fig. 3.8. These are the electron gun, the magnetic lens system, the electron collector, the visual and recording cathode ray tubes (CRT's) and the electronic console controlling them. Referring to this schema, the basic operating principles of the SEM can be summarily described as follows.

The electron gun provides a beam of electrons with energy adjustable between 1 and 30 kV. The condenser and objective lens system are used to demagnify the electron image formed at crossover in the electron gun into a small-diameter probe which is then scanned over the specimen. The condenser

lens determines the beam current that impinges on the sample, whereas the objective lens determines the final spot size of the electron beam.

Scanning of the specimen with the probe is performed through the scan coils that deflect the beam in a rectangular pattern. The scan generator which produces sweep signals to the scan coils, at the same time, operates the deflection coils of the CRT's. This synchronization results in a one-to-one correspondance between the position of the electron beam on the fracture surface and that of the spot on the cathode ray tubes.

The beam-sample interaction produces three main signals, namely, secondary electrons, primary back scatter electrons and X-rays that are processed through the SEM's electronics. The first two are mostly used when information about the specimen topography is needed, whereas the latter provides useful information about the composition of the specimen surface.

From the control console, the electron gun accelerating voltage, the lens current, the magnification and many other observation parameters can be adjusted.

3.5 TESTING PROCEDURE

3.5.1 Fatigue Experiments

After having gained experience with the operation of the MTS machine through several preliminary runs, a test protocol was established for the fatigue experiments. The highlights of this protocol are given below, with the detailed steps being enumerated in Appendix B.

Prior to the experiments, a general calibration check of all the electronic modules was performed following the procedures described in the MTS owner's reference manuals. Then, the recommended optimum hydraulic fluid temperature was reached by warming up the HPS unit with a low frequency low amplitude sine command signal sent to the actuator. Next the extensometer was installed on the specimen whose test section had been previously protected with some adhesive copper tape at the contacting points of the extensometer's knife edges. This was to prevent the fatigue crack from occurring at the knife edges due to indentation. The specimen installation in the load train was carried out in the load control mode, since it is recognized to be the safest mode for specimen mounting. A 3kN tensile load was then applied on the specimen for alignment purposes. After releasing this load, the system was switched to strain control and a programmed ± 0.30 percent strain at a frequency of 1 Hz was applied on the specimen. The test was stopped when complete fracture occurred. An electronic device (Fig. 3.9) was built and coupled with the limit detector module in order to switch the HPS unit off (and so doing, to stop the cycle counter) when separation of the specimen was detected. The broken specimens were finally put back in the plastic containers prior to the fractographic studies.

3.5.2 SEM Observations

The procedure for the SEM observations is only briefly described below. A detailed description as well as initial settings can be obtained from the user's manual [31].

For the microscopic observation, the sample was glued on a standard 12.7 mm diameter aluminum stub by means of a special non-volatile conductive cement and it was placed in the SEM vacuum chamber. A 1×10^{-5} torr vacuum was then created in the chamber and a 20 kV accelerating voltage was selected in the electron source module.

Starting at low magnification, the best image of the fracture surface was obtained by manipulating the focus and condenser controls, by adjusting contrast and brightness on the viewing CRT with the appropriate control buttons, and by adjusting the vertical position (Z-axis) of the specimen through the micrometric screw mounted on the vacuum chamber. Once a region of interest was found on the specimen surface, contrast and brightness on the recording CRT were separately adjusted with the aid of the corresponding controls and a picture was taken using the camera provided with the SEM.

CHAPTER 4

EXPERIMENTAL RESULTS AND THEIR INTERPRETATION

4.1 DATA PRESENTATION

At the end of the fatigue experiments, specimens that failed due to abnormal testing conditions such as excessive bending stress or fatigue cracks initiating in the vicinity of the clip-on-gage's knife edges, were eliminated. Thus, the results from 18 tests were retained for further analysis.

A median ranking [32] of the fatigue data was then performed since it was decided to fit the previously described cumulative distribution functions to the experimental data. The reasons for this choice are explained in the next section.

The test conditions are resumed in Table 4.1 as per the ASTM E468-76 standard, while the ranked experimental results are presented in Table 4.2 and plotted in Fig. 4.1.

4.2 STATISTICAL INTERPRETATION OF DATA

When one has to assess the reasonableness of a selected reliability model, two different approaches are usually considered: probability plotting and statistical tests.

Probability plotting is a simple visual method that shows how well the assumed distribution fits the data. It requires the use of probability paper especially designed for the distribution under examination. Since

this graph paper was not available for some of the investigated CDF's and because its construction would have been a very involved (if not impossible) task, it was decided to analytically curve fit the CDF's, except the "Provan law", to the fatigue data by estimating their respective parameters through whichever of the following methods was most appropriate; the matching moment method, the maximum-likelihood method and the least square method. These are briefly described in the Appendix C. In the case of the "Provan law", the function parameters were successively computer optimized to yield the best fit. The curve fit and plotting program listings are presented in the Appendix F.

The second approach, namely, the statistical tests, provides a probabilistic framework in which to evaluate the adequacy of the model and supplements the probability plots (CDF's curve fits in this case) when the latter fails to provide a clear cut decision. Statistical tests used in this investigation are further discussed in Section 4.3.1.

The following sections describe the particular method used to obtained each of the CDF fits.

4.2.1 Exponential

Recalling Eq. (2.3), we have for the exponential distribution:

$$\text{CDF} = 1 - e^{-N/\delta}$$

or:

$$1 - \text{CDF} = e^{-N/\delta}$$

where N represents the number of cycles to failure. Taking the logarithm

we obtain:

$$\ln (1-\text{CDF}) = -\frac{N}{\delta} , \quad (4.1)$$

which is the recognizable equation of the straight line $Y = AX$, with $Y = \ln(1-\text{CDF})$ and $A = -1/\delta$. A preliminary plot of the data points on a semi-log paper showed a very poor agreement with Equation (4.1). Therefore, a location parameter was included in the equation to get the best possible fit. This yielded:

$$\ln (1-\text{CDF}) = \frac{-N}{\delta} + \frac{\alpha}{\delta} , \quad (4.2)$$

or:

$$Y = AX + B$$

with A and B being evaluated by the method of least squares. The exponential fit is shown in Fig. 4.2 a).

4.2.2 Normal

The normal CDF given by Eq. (2.5), namely:

$$\text{CDF} = \frac{1}{\sigma\sqrt{2\pi}} \int_{-\infty}^N \exp\left[-\frac{1}{2}\left(\frac{\xi-\mu}{\sigma}\right)^2\right] d\xi ,$$

can also be expressed in terms of the complementary error function [26] as:

$$\text{CDF} = \frac{1}{2} \operatorname{erfc} \left(\frac{\mu-N}{\sigma\sqrt{2}} \right) . \quad (4.3)$$

After having evaluated the maximum likelihood unbiased estimators for μ and σ , namely:

$$\hat{\mu} = \frac{1}{n} \sum_{i=1}^n N_i, \quad \hat{\sigma} = \left(\sum_{i=1}^n \frac{N_i - \hat{\mu}}{n-1} \right)^{1/2}, \quad (4.4)$$

the normal curve fit depicted in Fig. 4.2 b) was computed by means of Eq. (4.2).

4.2.3 Log Normal

The method used to obtain the log normal fit illustrated in Fig. 4.3 a) is essentially the same as the one just described for the normal fit, except that the N_i 's in Eqs. (4.3) and (4.4) were replaced by their logarithm.

4.2.4 Gamma

Although there exist several methods to estimate the gamma parameters, for most engineering problems, especially when there are 20 or less data points, the matching moment method is simpler to apply and yields fairly good estimates. In this case, the expressions for the estimators are:

$$\hat{\lambda} = \frac{N(n-1)}{\sum (N_i - \bar{N})^2}; \quad \hat{\eta} = \hat{\lambda} \bar{N}, \quad (4.5)$$

where:

$$\bar{N} = \sum_{i=1}^n \frac{N_i}{n}$$

From these and using Eq. (2.17), the gamma fit shown in Fig. 4.3 b) was plotted.

4.2.5 Weibull (2-parameter)

A first plot of the data points on Weibull paper showed that they were relatively well described by a straight line. Therefore, there was no need to include a location parameter, that is, to use the 3-parameter Weibull CDF given by Eq. (2.22).

Hence, taking twice the logarithm of Eq. (2.20), namely:

$$\text{CDF} = 1 - \exp\left[-\left(\frac{N}{\theta}\right)^\beta\right],$$

we get:

$$\ln \ln \left(\frac{1}{1-\text{CDF}}\right) = \beta \ln N - \beta \ln \theta \quad (4.6)$$

which is again the equation of the straight line, $Y = AX + B$, with:

$$Y = \ln \ln \left(\frac{1}{1-\text{CDF}}\right),$$

$$A = \beta,$$

$$X = \ln N,$$

and: $B = -\beta \ln \theta.$

The parameters β and θ were evaluated by the least square method to obtain the 2-parameter Weibull CDF plot shown in Fig. 4.4 a).

4.2.6 Gumbel (Largest and Smallest Values)

In a similar procedure as for the Weibull fit, Eqs. (2.23) and (2.25), namely:

$$CDF = 1 - \exp[-\exp(\frac{N-\alpha}{\delta})] ,$$

$$CDF = \exp\{-\exp[-(\frac{N-\alpha}{\delta})]\} ,$$

are converted into the following straight line forms:

$$\ln \ln \left(\frac{1}{1-CDF} \right) = \frac{N}{\delta} - \frac{\alpha}{\delta} , \quad (4.7)$$

$$\ln \ln \frac{1}{CDF} = -\frac{N}{\delta} + \frac{\alpha}{\delta} . \quad (4.8)$$

From these, the parameters δ and α were computed which then yielded the plots of the Gumbel largest value and smallest value fits, illustrated in Figs. 4.4 b) and 4.5 a), respectively.

4.2.7 Birnbaum-Saunders

Defining:

$$S = \frac{1}{n} \sum_1^n N_i ; \text{ and } R = \left(\frac{1}{n} \sum_1^n \frac{1}{N_i} \right)^{-1} , \quad (4.9)$$

Birnbaum and Saunders find [33] that for small values of α , the relation:

$$\hat{\beta} = \sqrt{SR} ,$$

yields an estimate of β close to the maximum-likelihood estimator. Then, α can be inferred from:

$$\hat{\alpha} = \left(\frac{S}{\hat{\beta}} + \frac{\hat{\beta}}{R} - 2 \right)^{1/2} . \quad (4.10)$$

The estimators $\hat{\beta}$ and $\hat{\alpha}$ were used in Eq. (2.32) to get the Birnbaum-Saunders CDF plot presented in Fig. 4.5 b).

4.2.8 "Provan"

The parameters, μ_{a_0} , V_{ac} and λ of the "Provan" cumulative distribution function, namely:

$$CDF = \frac{1}{2} \left\{ \operatorname{erf} \left(\frac{\mu_{a_0} e^{\lambda N} - \mu_{af}}{\sqrt{2V_{ac}}} \right) + \operatorname{erf} \left(\frac{\mu_{af}}{\sqrt{2V_{ac}}} \right) \right\},$$

were optimized by means of an iterative procedure to minimize the RMS error. Starting values for μ_{a_0} and V_{ac} were taken from the results of previous experiments [21]. The value for μ_{af} , the final mean crack length, was set equal to the specimen diameter since the fatigue tests were stopped when complete separation of the specimen occurred. The "Provan" CDF plot is shown in Fig. 4.6.

4.3 COMMENTS AND COMPARISONS

4.3.1 CDF Curves

4.3.1.1 Curve Fitting

As a comparison criterion, a root mean square error was calculated for each fit by means of the relation:

$$ERROR_{RMS} = \left[\frac{1}{n} \sum_{i=1}^n (E_i)^2 \right]^{1/2}, \quad (4.11)$$

where n is the number of data points (i.e., $n = 18$) and E_i is the error for the data point i and is given by the differences between the observed (i.e., ranked) probability and the computed (i.e., best fit) probability of failure.

The nine investigated laws are listed in Table 4.3 with their computer-estimated parameters and their corresponding error given by Eq. (4.11). One can see from this table that the exponential law yields a poor fit compared to the other laws. The normal CDF appears to give the best fit and the log normal, the gamma, the 2-parameter Weibull and the Birnbaum-Saunders laws follow with roughly the same error. Finally, the Gumbell largest and smallest values laws and the "Provan law" describe the data with approximately the same degree of goodness-of-fit, the "Provan" fit being relatively poor at the tails of the distribution. The above observations can be visualized from the curves shown in Fig. 4.2 through 4.6.

4.3.1.2 Statistical Tests

In addition to the curve fitting method, two statistical tests namely, the Kolmogorov-Smirnov test [34] and the Cramer-Von Mises test [35] were performed on the assumed CDF's to assess their validity as failure models with respect to the available data.

Before applying the tests, the null hypothesis was defined as follows:

H_0 : the set of data is a sample from the assumed distribution

Furthermore, the level of significance, α , that is, the probability of rejecting the null hypothesis when the latter is true, was chosen to be .05.

The Komolgorov-Smirnov test statistic was first calculated with:

$$D = \text{Max}_{\text{all } i} |(F(N_i) - S(N_i))| , \quad (4.12)$$

where

$F(N_i)$ = the assumed cumulative distribution function, and
 $S(N_i)$ = the sample cumulative distribution function
(i.e., the rank) at $N = N_i$.

The test statistic given by Eq. (4.12) was then compared with a critical (maximum allowable) value obtained from [36] and referenced by the sample size and the chosen level of significance.

After having arranged the sample data in increasing order, the Cramer-Von Mises test statistic was evaluated through:

$$n\omega^2 = \frac{1}{12n} + \sum_{i=1}^n \left[\frac{2i-1}{2n} F(N_i) \right]^2 , \quad (4.13)$$

which is an approximation, for a small sample of size n , of the exact test statistic defined by:

$$\omega^2 = \int_{-\infty}^{\infty} [F(N) - S(N)]^2 dF(N) , \quad (4.14)$$

Again the test statistic was compared to a critical value [36] corresponding to a .05 level of significance.

The results of the statistical test are presented in Table 4.4. This table shows that the hypothesis of exponential distribution is rejected by both tests whereas the null hypothesis for all the other distributions is accepted which, however, does not imply that they are verified. This only means that because of a limited number of data, one cannot dismiss the possibility that the assumed underlying statistical failure model be, with the exception of the exponential law, any of the reliability laws under investigation.

4.3.2 The Fatigue Transition Intensity (λ)

In this section are briefly described three different methods used to determine the major parameter of the "Provan law", namely, the transition intensity, λ . The resulting λ 's were compared in order to ascertain the applicability of the "Provan law" as a fatigue reliability model which was the prime interest of the current study.

A theoretical interpretation of the transition intensity, λ_{th} , was first determined through an iteration procedure detailed in [20]. This procedure essentially utilizes two points on the Wohler "S-N" curve pertaining to the polycrystalline metal under investigation. In the present study of OFHC copper, one of these points corresponded to a 0.003 strain amplitude while the other was taken as corresponding to the mean value of the results of two fatigue tests performed at a strain amplitude of 0.0015.

Second, an experimental value, λ_{exp} , was evaluated for the transition intensity using a procedure again detailed in [20]. This experimental evaluation mainly consists of counting the fatigue striations and their spacings on a fractograph of the specimen surface and in evaluating the transition intensity from the resulting statistics. These are the mean crack length, μ_{a_i} , for a given cycle and the corresponding crack growth rate $\frac{d\mu_{a_i}}{di}$ which are related to the transition intensity as follows:

$$\frac{d\mu_{a_i}}{di} = \lambda \mu_{a_i} \quad (4.15)$$

Typical fractographs used for striation counting are shown in Figs. 4.7 to 4.9.

Finally, an empirical transition intensity, λ_{emp} , was determined by curve fitting the "Provan law" to the fatigue data using the optimization procedure previously described in Section 4.2.8.

The three resulting values for the transition intensity are given in Table 4.5. The discrepancy between the theoretical and experimental values, already noted in [20], is again observed here which tends to indicate the inadequacy of the Markovian crack growth model in describing the fatigue mechanism. This is further discussed in the conclusions.

One also finds a disparity of almost an order of magnitude between the experimental and empirical values for λ . However, during the fatigue experiments it was generally observed that the crack initiation period represented nearly 80% (and up to 90% in some cases) of the total life of

the specimens. Thus, λ_{emp} being calculated for the total number of cycles to failure, one should expect, for a similar curve fit of Eq. (2.42), a transition intensity much closer to the experimental value if only the number of cycles for propagation is considered. This inability of distinguishing between fatigue cycles involved in initiating a crack from those involved in its propagation is further discussed in the recommendations for further research section of this thesis.

CHAPTER 5

CONCLUSIONS

5.1 CONCLUDING REMARKS

This thesis aimed at experimentally evaluating the adequacy of certain fatigue reliability laws with the attention being focused on the "Provan law" that has recently been derived based upon a probabilistic micromechanics representation of the fatigue crack growth in polycrystalline metals. From the analysis of the resulting data the following conclusions are drawn:

1. All the reliability laws tested in the present investigation, with the exception of the exponential law, appear to give a fairly good description of the scatter in the available fatigue data. However, the number of these data being small, the statistical tests used in the analysis fail to identify which of the reliability distributions is (or are) the most appropriate. Furthermore, it was observed that the empirical and semi-empirical laws fit the data as adequately as (if not better than) the Birnbaum-Saunders and the "Provan" laws which both ensued from microstructural modelling of the fatigue degradation process. This tends to support the assertion that in some cases, although there is no theoretical justification for using a particular reliability model, the latter can be considered acceptable based only on the empirical approximation it provides. Nevertheless, we should always keep in mind that the most suitable reliability law is obtained when the failure data *and* the understanding of the physical processes causing failure, complement each other.

2. The "Provan" fatigue reliability law can be used in an *empirical fashion*, that is, without any reference to any microstructural information, provided one is not particularly concerned about what happens at the tails of the distribution. This is certainly a positive conclusion from the engineer's point of view but a rather unsatisfactory one from the researcher's. In fact, a comparison of the different values obtained in the present investigation for the crack growth transition intensity, λ , clearly indicates that the Markov linear birth model, the theoretical basis of the "Provan law", underestimates the crack growth rate and, therefore, does not provide an adequate description of the fatigue process.

5.2 PROPOSALS FOR FURTHER RESEARCH

In the light of the results presented in this thesis there is an obvious need to seriously review the theoretical development leading to the "Provan law" before it can be confidently applied to fatigue reliability. In that sense, Markov stochastic processes other than the linear pure birth process should be investigated, recalling that the main disadvantage of the latter is that it does not take into consideration the spatial correlation of the material points along the crack front.

It is also the author's hope that an improved probabilistic micro-mechanics fatigue model will enable one to solve the age old problem as to correctly assess the number of cycles involved in the crack initiation process and in the subsequent propagation process. This was, indeed, the main reason for the discrepancy between the three values of λ evaluated in the present investigation.

During the last few years we have seen an increasing use of probabilistic models for predicting the performance of components and large engineering systems. The "Provan law" ensues from one of these models and when it becomes operational, from the design point of view, one will be able to perform a fatigue reliability analysis on the basis of a Markovian law, material properties obtained in a laboratory, and only a few fatigue tests. Thus, cumbersome and expensive experiments that are currently used and often yield unsatisfactory results will no longer be required.

REFERENCES

1. Weibull, W., "A Statistical Representation of Fatigue Failure in Solids", Acta Polytech, Mech. Eng. Serv., Vol. 1, No. 9, (1949).
2. Leiblein, J. and Zelen, M., "Statistical Investigation of the Fatigue Life of Deep-Groove Ball Bearings", Journal of Research, National Bureau of Standards, Vol. 57, pp. 273-316, (1956).
3. Kao, J.H.K., "A New Life Quality Measure for Electron Tubes", IRE Trans., Reliability Quality Control, No. 7, p. 1, (1956).
4. Perry, J.N., "Semiconductor Burn-in and Weibull Statistics", Semiconductor Reliability, Vol. 2, Engineering Publishers, Elisabeth, New York, pp. 80-90, (1962).
5. Epstein, B., "The Exponential Distribution and its Role in Life-Testing", Industrial Quality Control, Vol. 15, No. 6, pp. 2-7, (1958).
6. Davis, D.J., "An Analysis of Some Failure Data", Journal of the American Statistical Association, Vol. 47, pp. 150-173, (1952).
7. Barlow, R.E. and Proschan, F., "Mathematical Theory of Reliability", John Wiley & Sons, New York, (1965).
8. Goldthwaite, L., "Failure Rate Study for the Log Normal Lifetime Model", Proceedings of the Seventh National Symposium on Reliability and Quality Control, pp. 208-213, (1961).
9. Howard, B.T. and Dobson, G.A., "High Stress Aging to Failure of Semiconductor Devices", Proceedings of the Seventh National Symposium on Reliability and Quality Control, (1961).
10. Peck, D.S., "Uses of Semiconductor Life Distributions", Semiconductor Reliability, Vol. 2., Engineering Publishers, Elisabeth, New York, pp. 10-28, (1962).
11. Gupta, S., "Order Statistics from the Gamma Distribution", Technometrics, Vol. 2, pp. 243-262, (1962).
12. Gumbel, E.S., "Statistical Theory of Extreme Value and Some Practical Applications", Nat. Bur. Std., Applied Mathematics, Ser. 33, (1954).
13. Hahn, G.J. and Shapiro, S.S., "Statistical Models in Engineering", John Wiley & Sons, New York, (1967).
14. Mann, N.R., Schafer, R.E. and Singpurwalla, N.D., "Methods for Statistical Analysis of Reliability and Life Data", John Wiley & Sons, New York, (1974).

15. Birnbaum, Z.W. and Saunders, S.C., "A New Family of Life Distributions", Journal of Applied Probability, Vol. 6, pp. 319-327, (1969).
16. Birnbaum, Z.W. and Saunders, S.C., "A Probabilistic Interpretation of Miner's Rule", SIAM Journal of Applied Probability Mathematics, Vol. 16, pp. 637-652, (1968).
17. Freudenthal, A.M. and Shinozuka, M., "Structural Safety under Conditions of Ultimate Load-Failure and Fatigue", WADD Technical Report, pp. 61-77, (1961).
18. Payne, A.D., "A Reliability Approach to the Fatigue of Structure", Probabilistic Aspect of Fatigue, ASTM STP 511, pp. 106-155, (1972).
19. Provan, J.W., "A Fatigue Reliability Distribution Based on Probabilistic Micromechanics", in: Sih, G.C. and Matczynski, M. (eds.), Proc. Defects and Fracture Symposium, Tuczno, Poland, (Oct. 1980).
20. Provan, J.W., "The Micromechanics Approach to the Fatigue Failure of Polycrystalline Metals", in: Gittus, J. (ed.), Voids, Cavities and Cracks in Metallic Alloys (Elsevier's Applied Science, 1981).
21. Mbanugo, C.C.I., "Stochastic Fatigue Crack Growth - An Experimental Study", Ph.D. Thesis, McGill University, Montreal, (1979).
22. Kao, J.H.K., "Statistical Models in Mechanical Reliability", Proceedings of the Eleventh National Symposium on Reliability and Quality Control, pp. 240-247, (1965).
23. Pearson, K., "Tables of the Incomplete Gamma Function", Biometrika Office, University College, London, (1957).
24. Cramer, H., "Mathematical Methods of Statistics", Princeton University Press, Princeton, N.J., (1964).
25. Gumbel, E.S., "Statistics of Extremes", Columbia University Press, New York, (1958).
26. Ghonem, H., "Stochastic Fatigue Crack Initiation and Propagation in Polycrystalline Solids", Ph.D. Thesis, McGill University (1978).
27. Provan, J.W., "Functional Analytic and Probabilistic Foundations in Solid Mechanics and Material Science", Lecture Notes, McGill University, (1976).
28. "OFHC Brand Copper - A Survey of Properties and Applications", AMAX Copper Inc., (1974).
29. "Constant Amplitude Axial Fatigue Tests of Metallic Materials", ASTM E466 Standard Recommended Practice, approved June 11, (1976).

30. Reference Manuals for the MTS 810.12 Closed-Loop Electro Hydraulic Testing System, MTS Systems Corporation, Minnesota, (1980).
31. User's Manual for the Scanning Electron Microscope, ETEC Corporation, California, (1974).
32. Lipson, C., and Narendra, J.S., "Statistical Design and Analysis of Engineering Experiments", McGraw-Hill Book Co., New York, (1973).
33. Birnbaum, Z.W. and Saunders, S.C., "Estimation for a Family of Life Distributions with Applications to Fatigue", Journal of Applied Probability, Vol. 6, pp. 328-347, (1969).
34. Marrey, F.S. Jr., "The Komolgorov-Smirnov Test for Goodness-of-fit", Journal of American Statistics Association, No. 4, p. 68-78, (1951).
35. Lindgren, B.W., "Statistical Theory", The Macmillan Company, New York, pp. 322-335 (1968).
36. Phillips, D.T., "Applied Goodness of Fit Testing", Monograph presented to the American Institute of Industrial Engineers Inc., (1972).

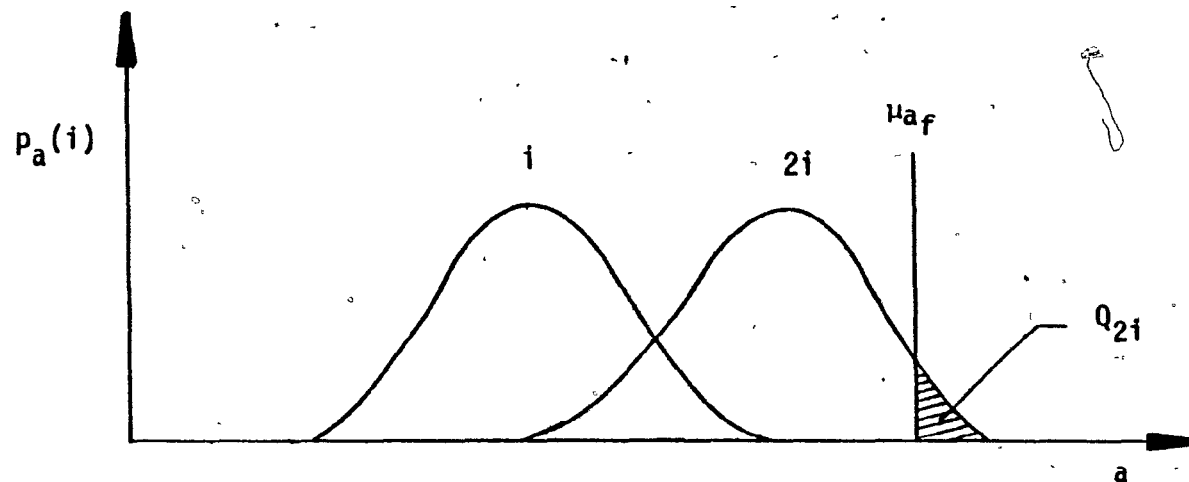
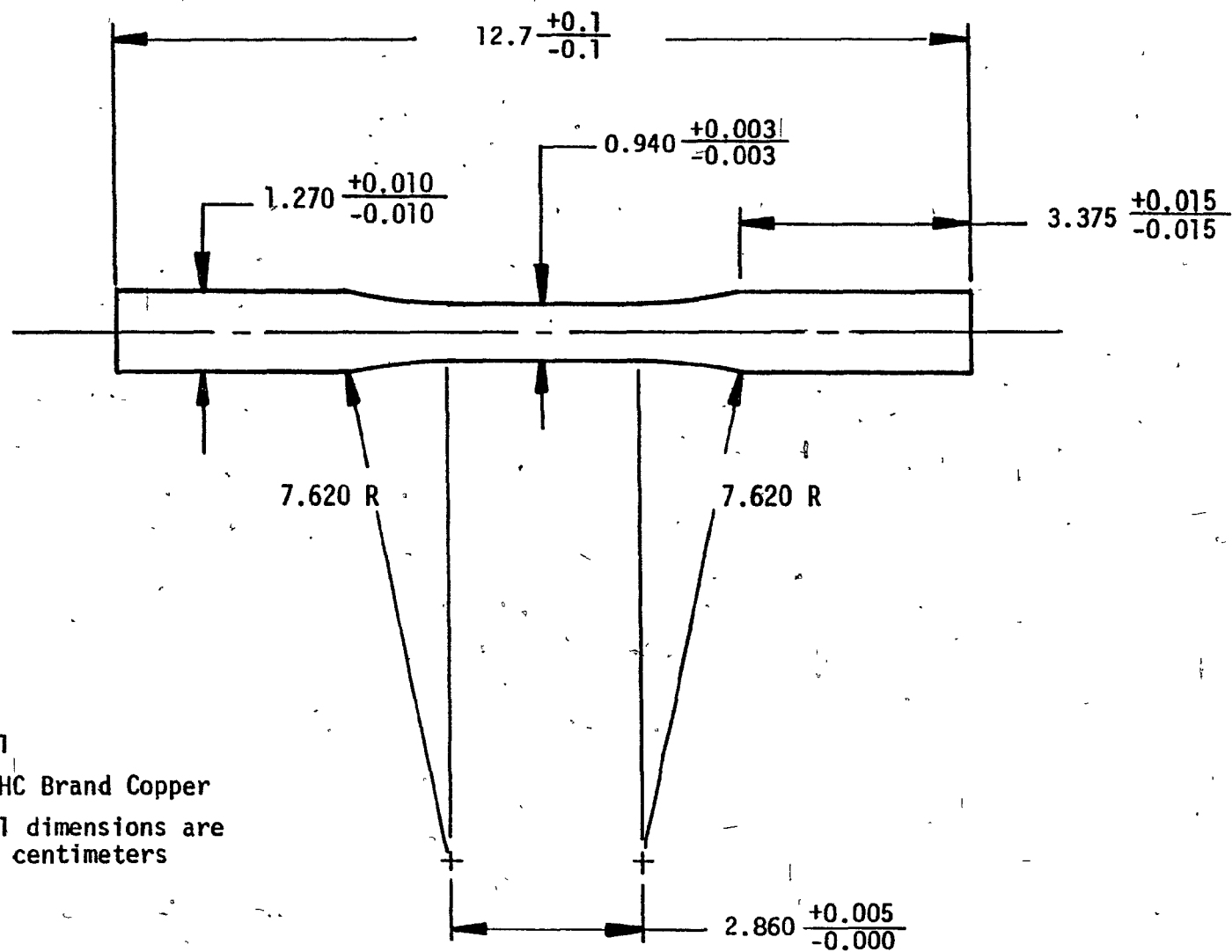


Fig. 2.1 Crack interference model leading to the "Provan" reliability law.



Scale: 1/1
 Material: OFHC Brand Copper
 Note: All dimensions are
 in centimeters

Fig. 3.1 Fatigue specimen with tangentially blending fillets.

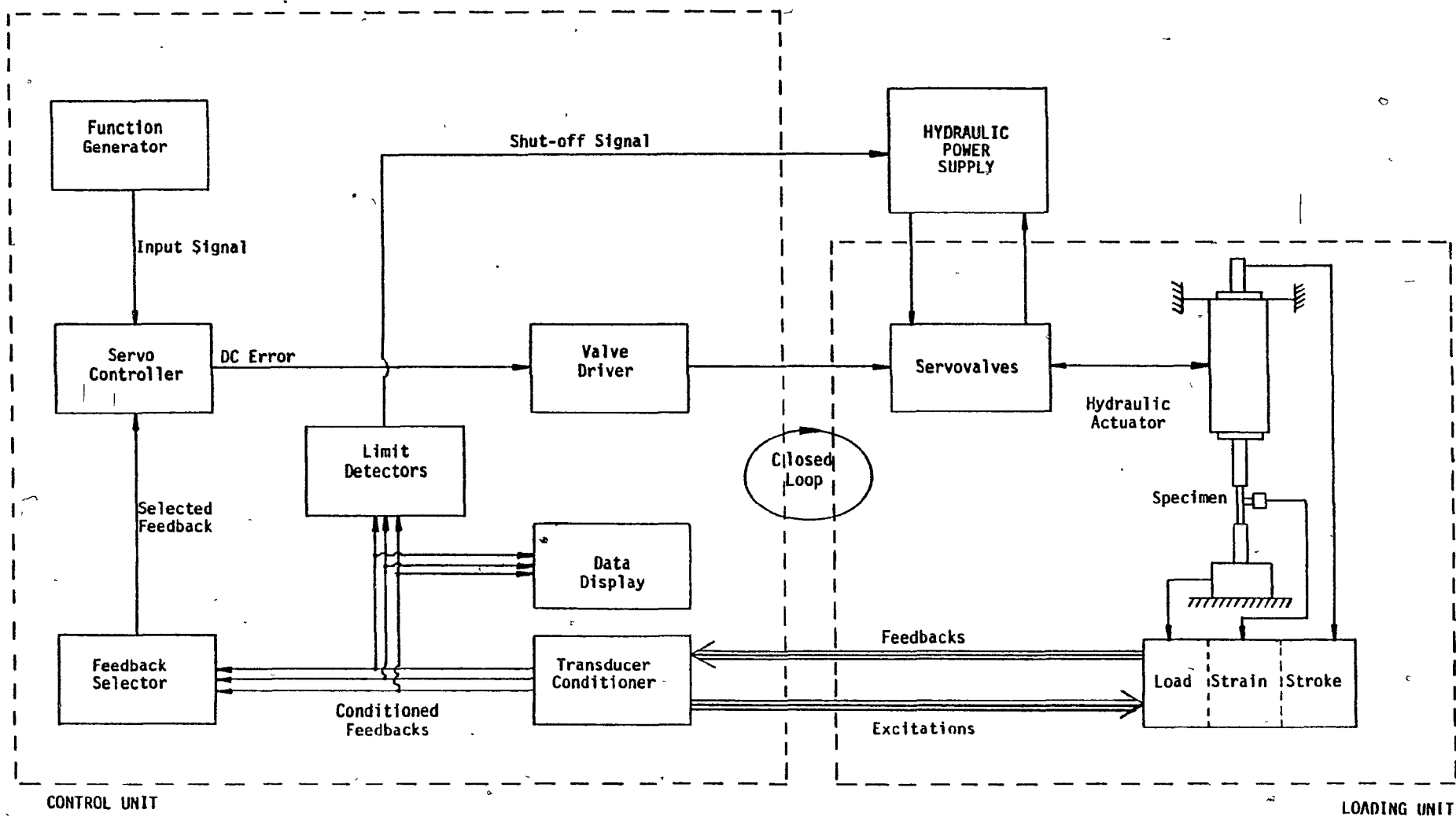


Fig. 3.2 Block diagram of the MTS test system.



Fig 3.3 Hydraulic power unit of the MTS testing system.

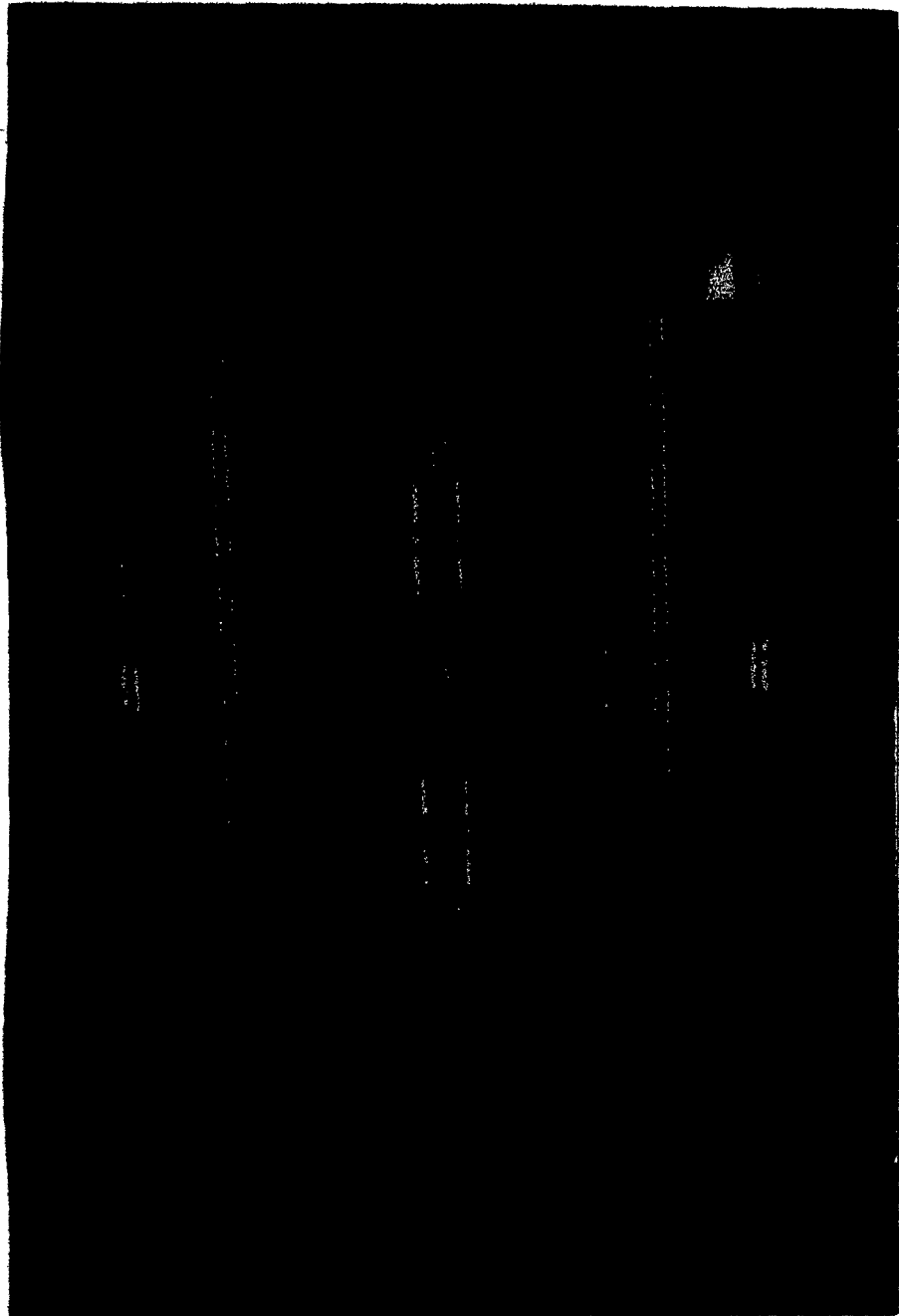


Fig. 3.4 Loading unit of the MTS testing system.

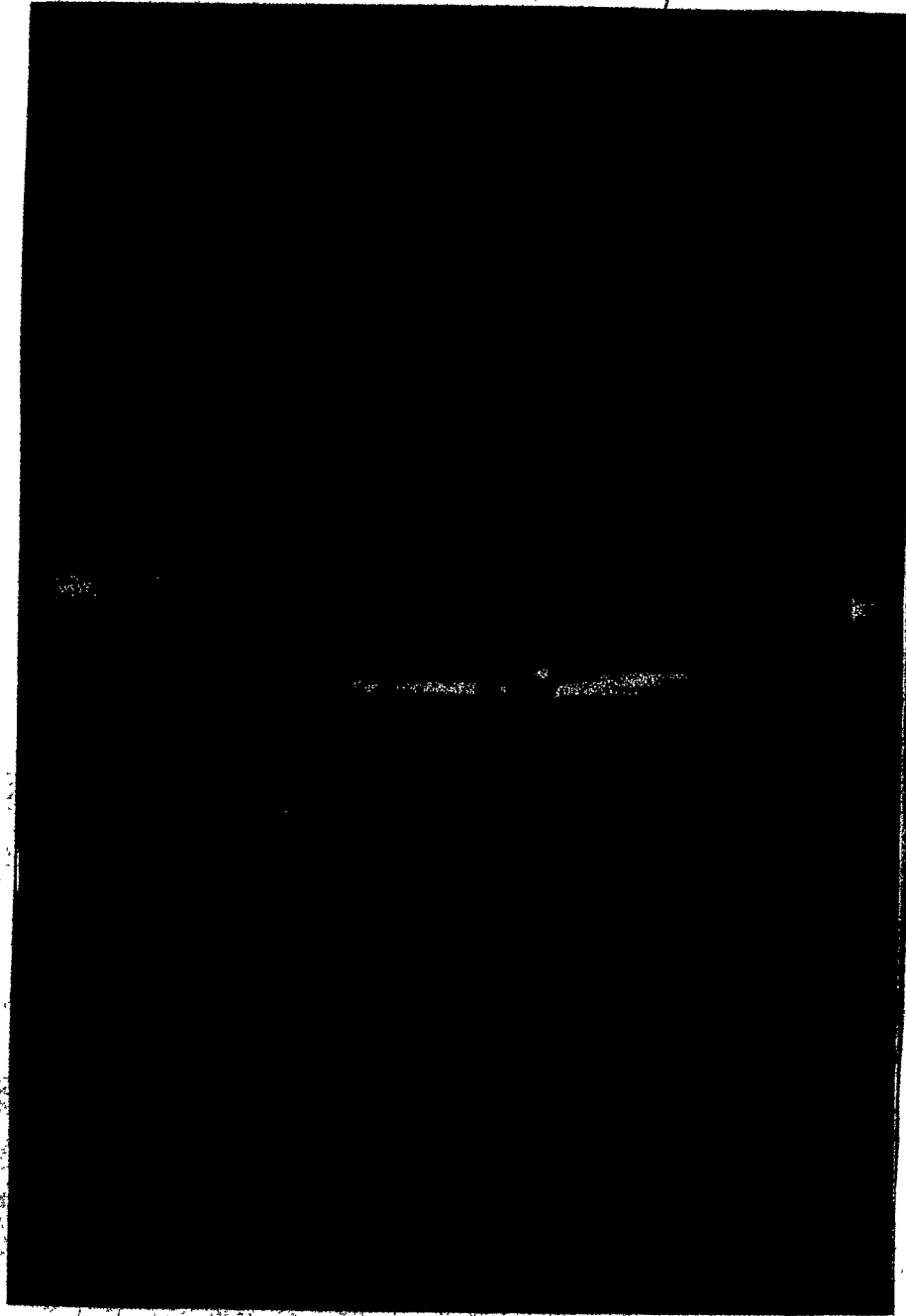


Fig. 3.5 The MTS axial extensometer.



Fig. 3.6 Control console of the MTS testing system.

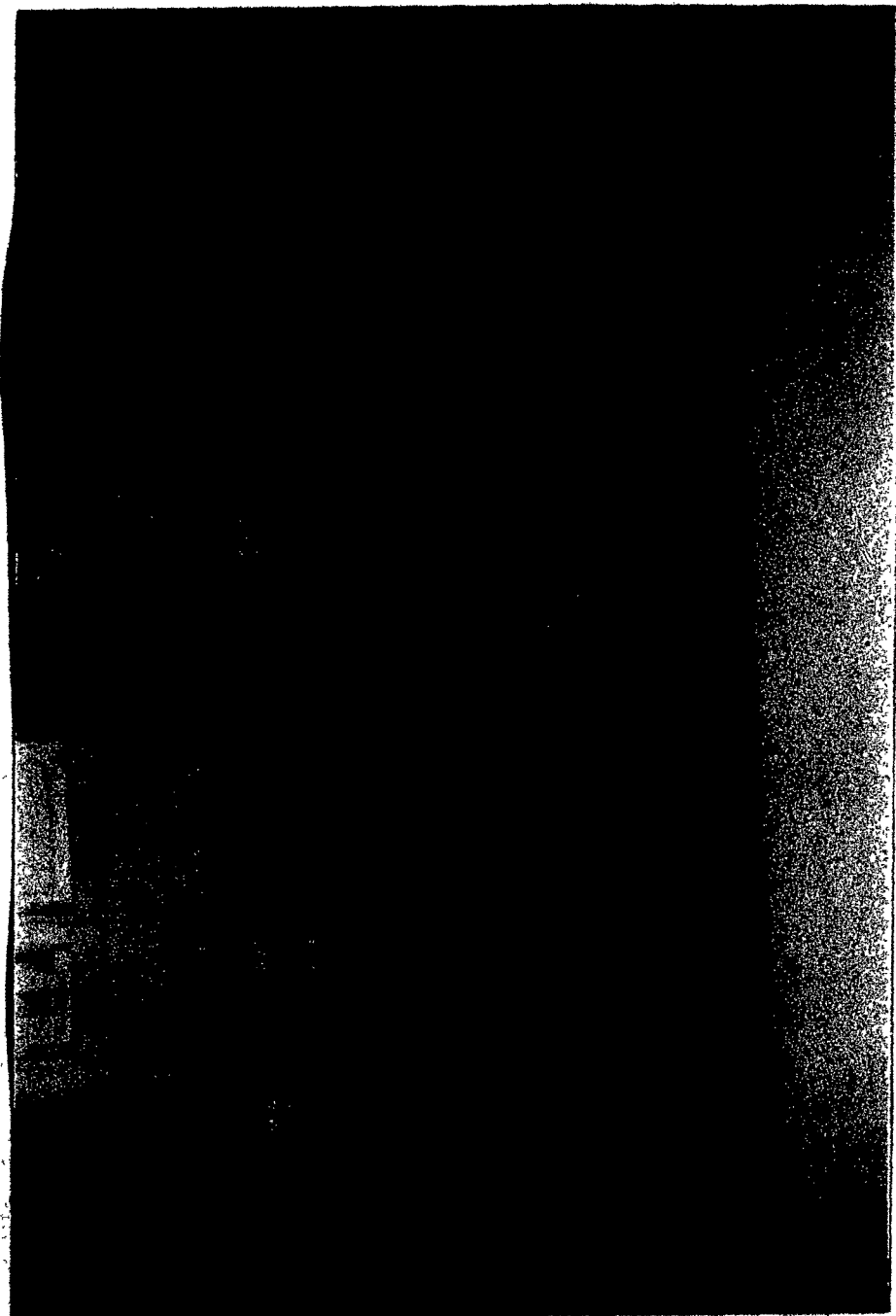


Fig. 3.7 Scanning electron microscope.

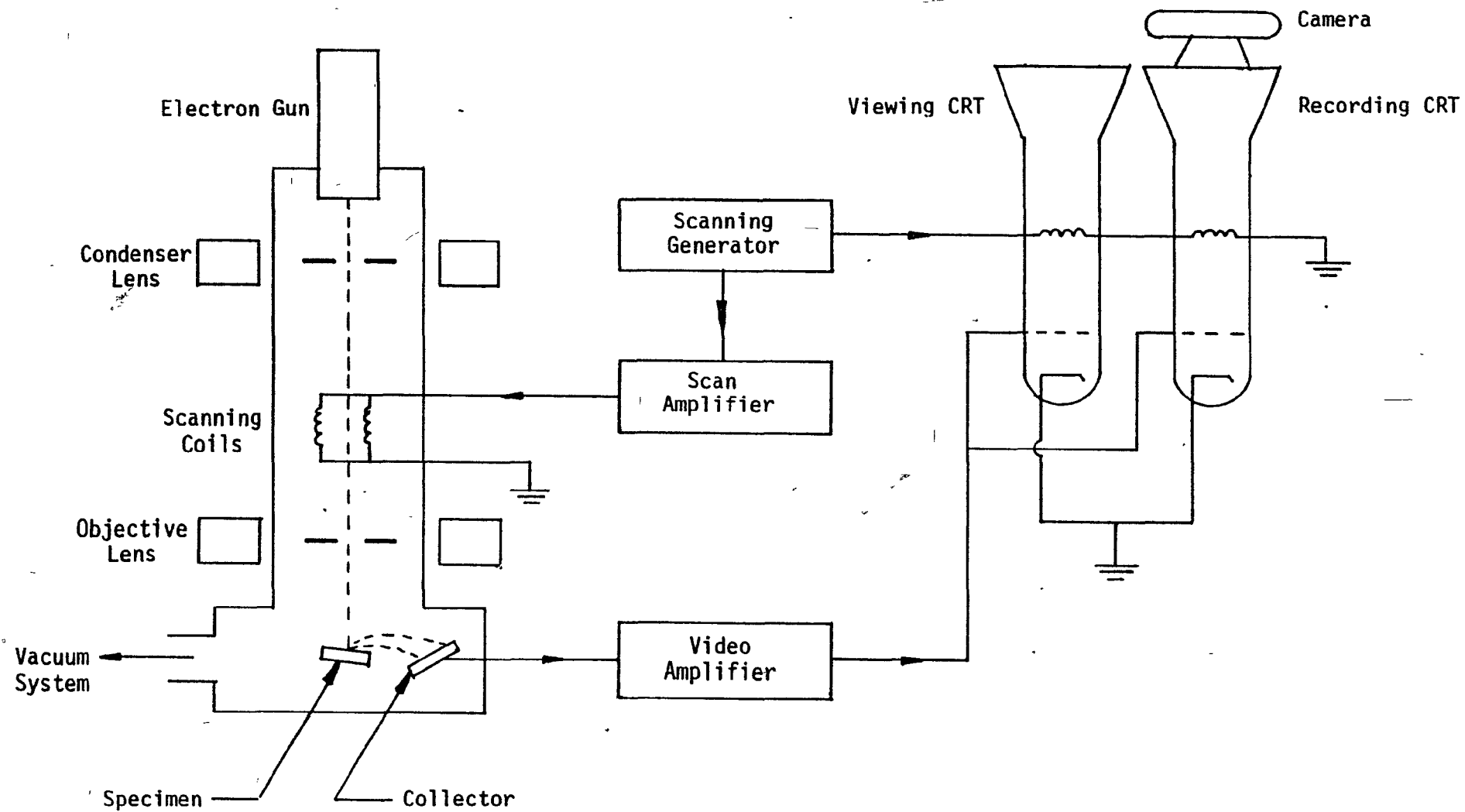
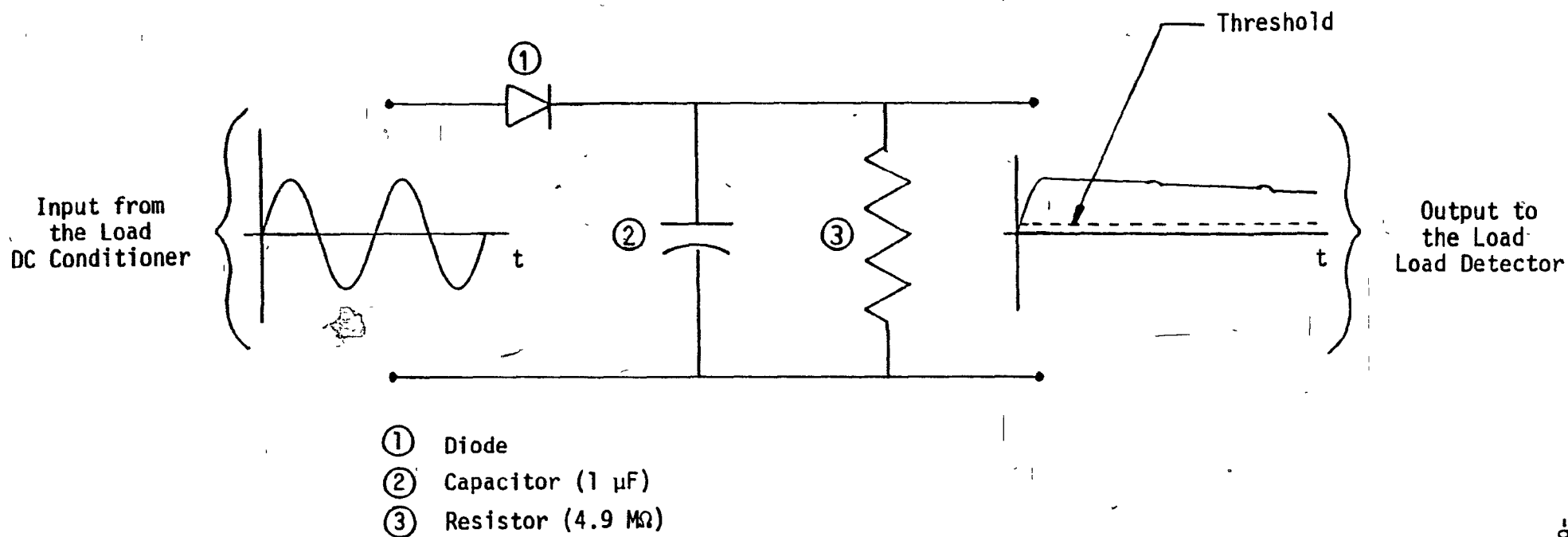


Fig. 3.8 Schematic of the scanning electron microscope.



- Operation:
1. As the fatigue crack propagates the load input signal decreases.
 2. The rectified output signal decreases accordingly until it reaches the threshold of the limit detector.
 3. The HPS unit is immediately shut off.

Fig. 3.9 Filtering circuit to detect specimen failure.

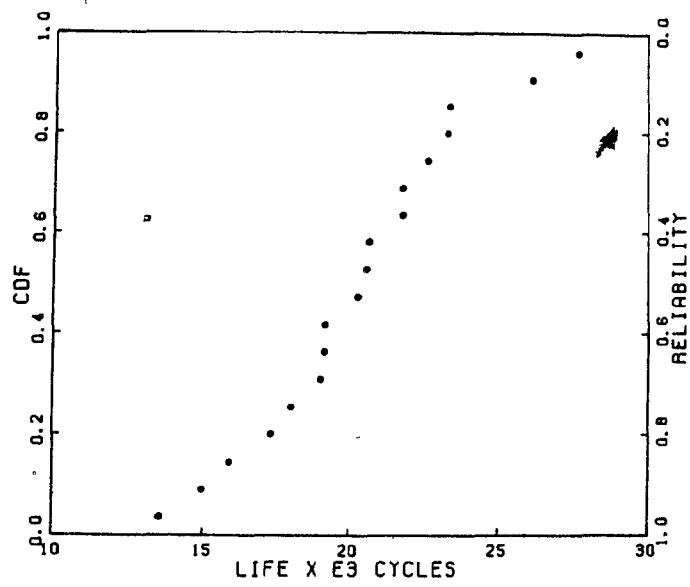
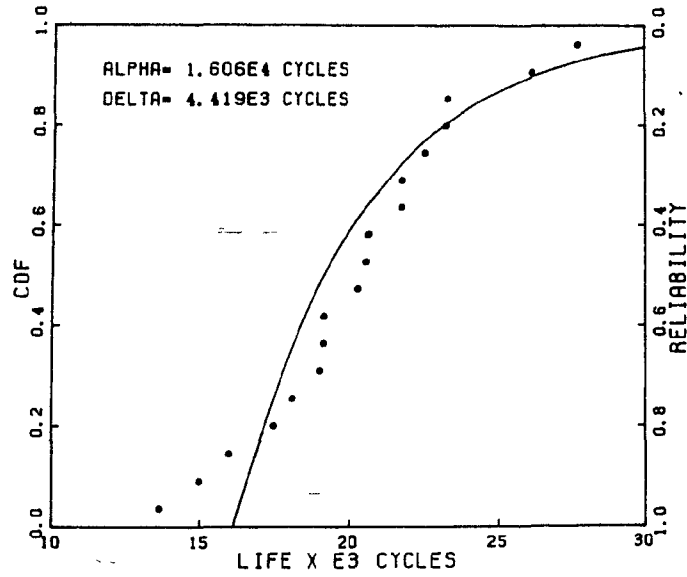


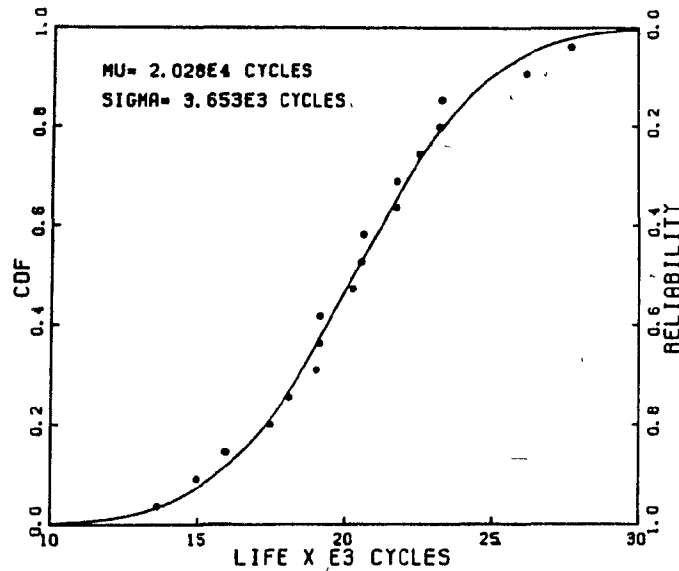
Fig. 4.1 Plot of the ranked experimental data.

EXPONENTIAL



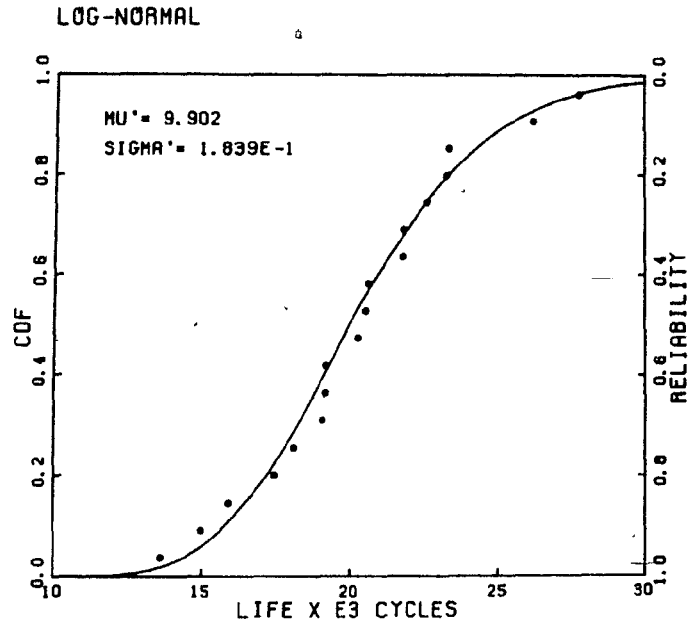
(a)

NORMAL

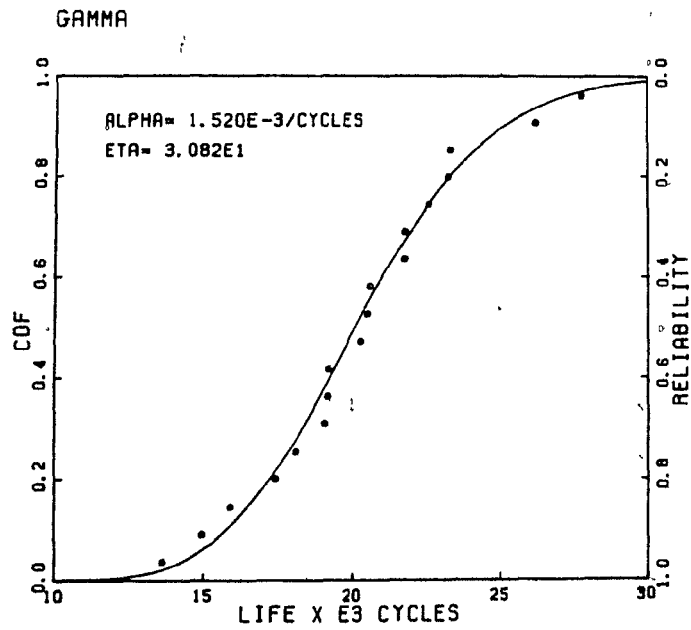


(b)

Fig. 4.2 a) Exponential, and b) normal CDF curve fits of the experimental data.

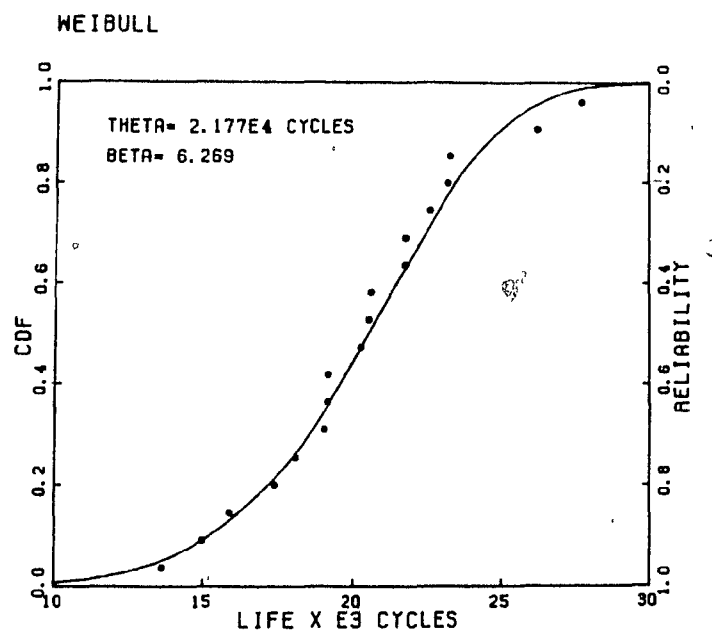


a)

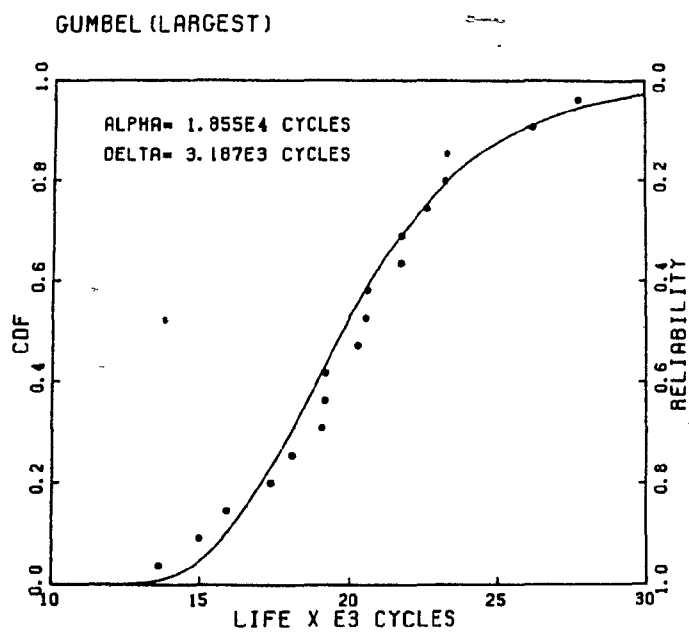


b)

Fig. 4.3 a) Log normal, and b) gamma CDF curve fits of the experimental data.



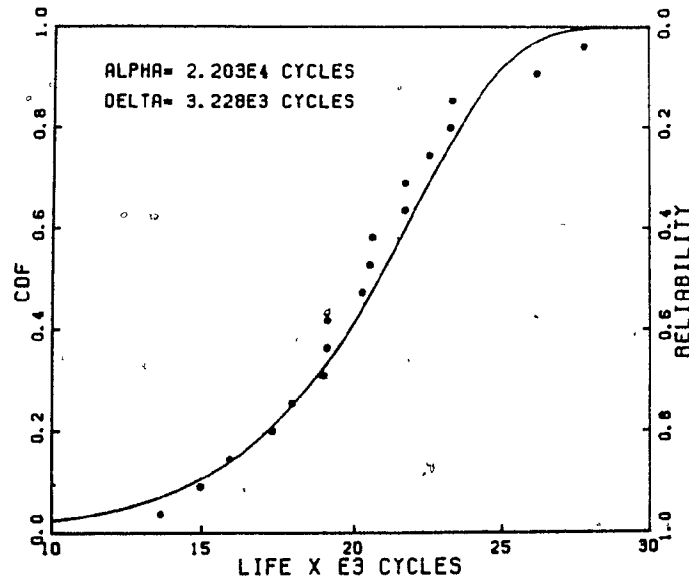
(a)



(b)

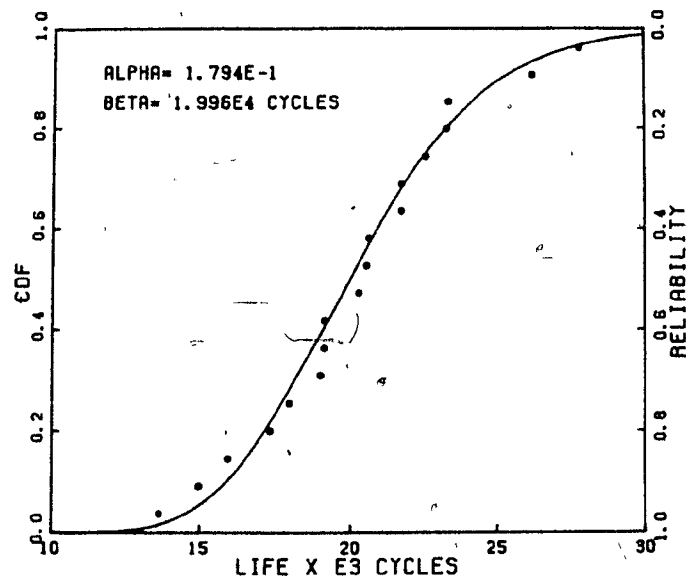
Fig. 4.4 a) Weibull, and b) Gumbel (largest value) CDF curve fits of the experimental data.

GUMBEL (SMALLEST)



(a)

BIIRNBAUM-SAUNDERS



(b)

Fig. 4.5 a) Gumbel (smallest value) and b) Birnbbaum-Saunders CDF curve fits of the experimental data.

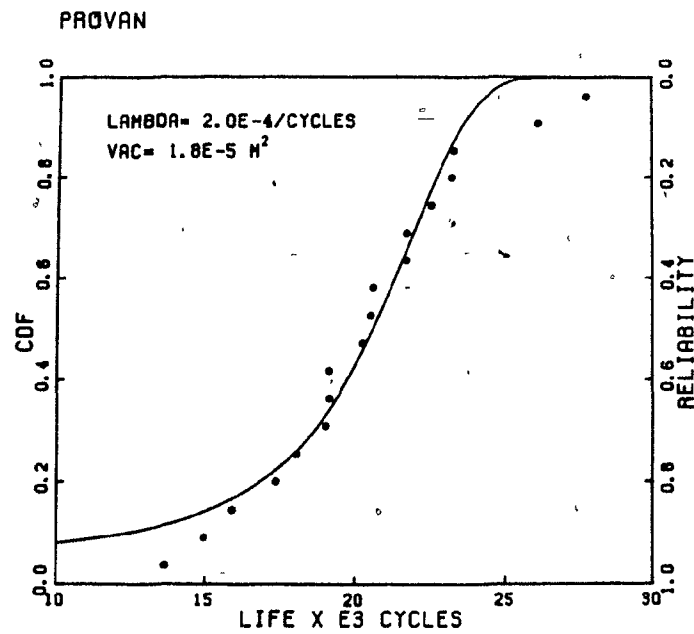


Fig. 4.6 "Provan" CDF curve fit of the experimental data.

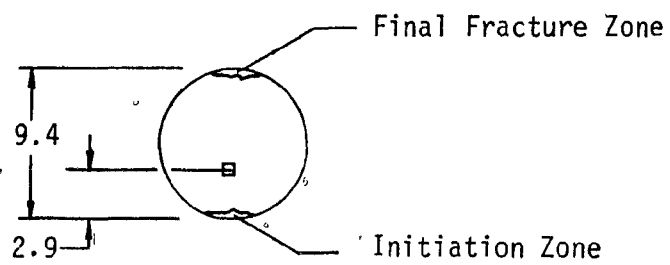
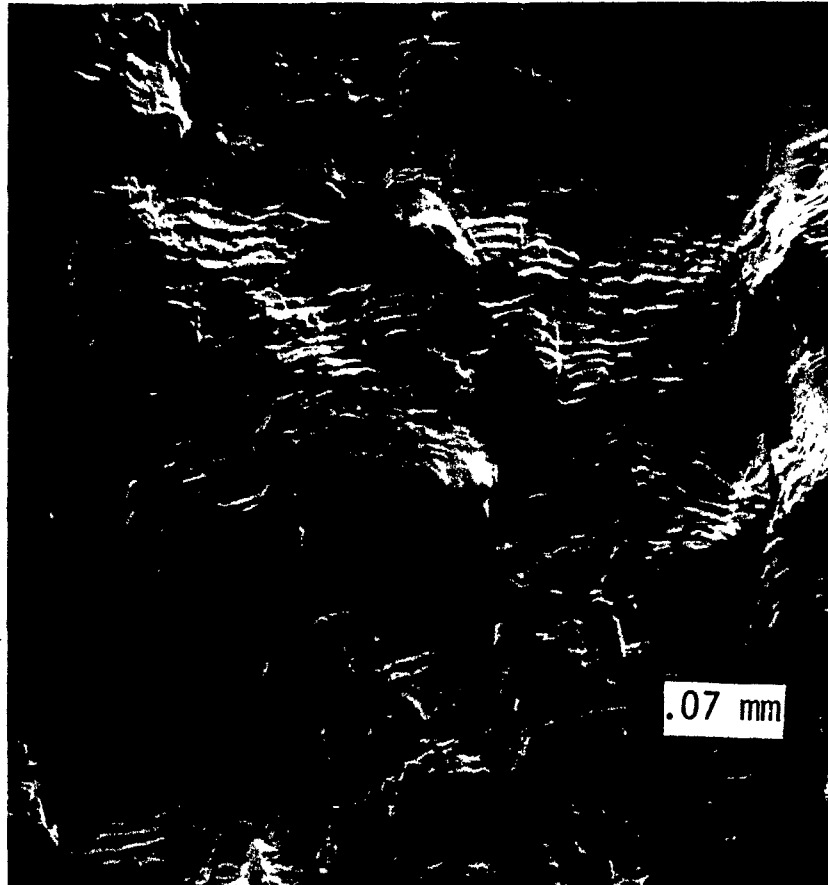
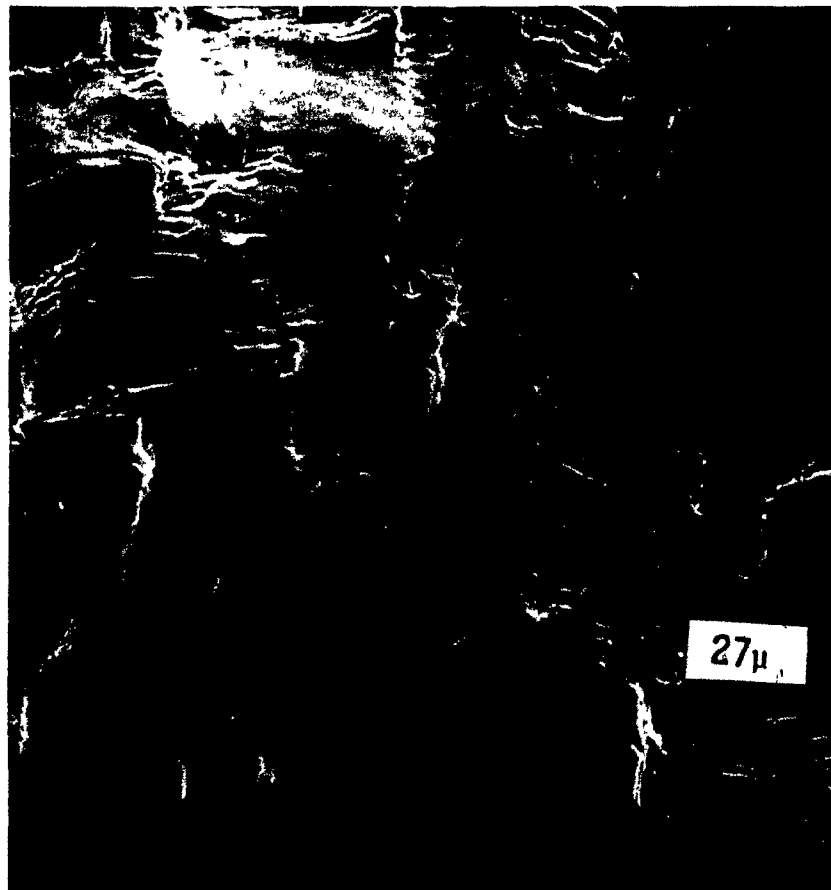


Fig. 4.7 Typical fractograph for OFHC copper.
(Region at 2.9 mm from the initiation zone.)



Fif. 4.8 Fractograph for OFHC copper.
(Region at 1.7 mm from the
initiation zone.)

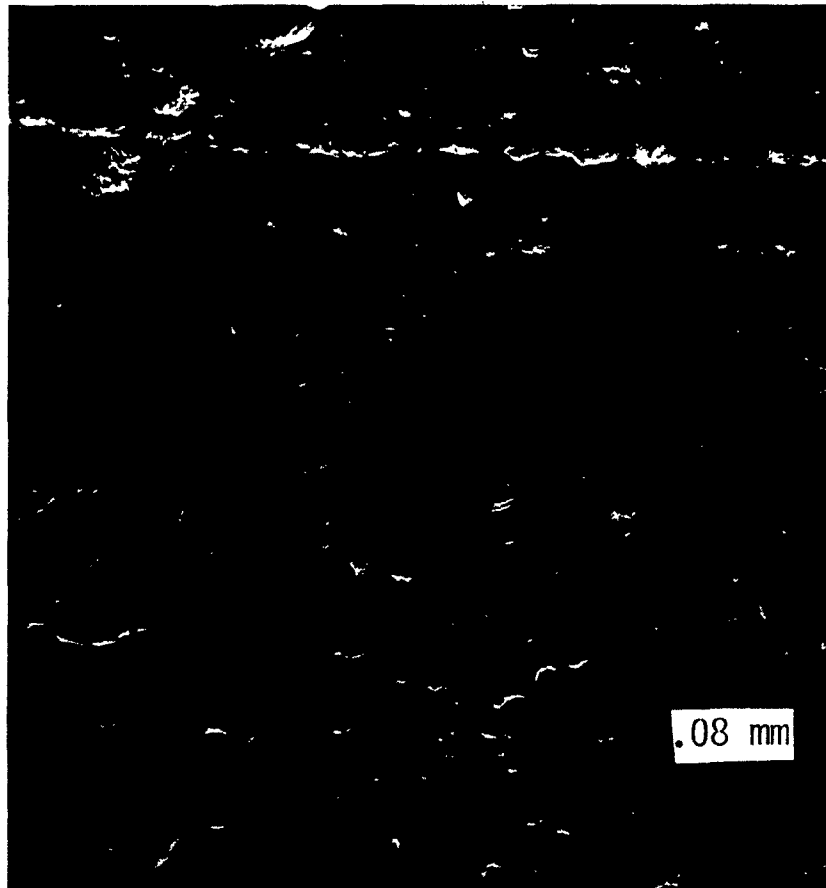


Fig. 4.9 Fractograph for OFHC copper.
(Region near the final fracture
zone.)

Distribution	Comments
Exponential	<ul style="list-style-type: none"> - probability distribution of life when a constant conditional failure (or hazard) rate, λ, is assumed - more appropriate for complex systems or assemblies - special case of Weibull and Gamma distributions
Normal	<ul style="list-style-type: none"> - applicable as a time to failure model if $\mu \geq 3\sigma$ otherwise, density function must be truncated - symmetric distribution without shape parameter
Log Normal	<ul style="list-style-type: none"> - derived from the consideration of analytical process wherein failure is due to the growth of a fatigue crack
Gamma	<ul style="list-style-type: none"> - time-to-failure distribution of a system if system failure occurs as soon as K independent subfailures have taken place at a constant rate α.
Weibull (2 parameters)	<ul style="list-style-type: none"> - widest applicability of all failure distributions - more appropriate to represent the life distribution of parts or components
Weibull (3 parameters)	<ul style="list-style-type: none"> - same comments as for 2-parameter Weibull - also known as the Type III asymptotic distribution for minimum values - for cases where the lower bound life is non-zero.
Gumbel (largest value) Gumbel (smallest value)	<ul style="list-style-type: none"> - also known as the Type I asymptotic distribution for maximum (largest) or for minimum (smallest) values - applicable whenever failure depends on the largest or smallest value of a variable (e.g., strength or flaw size) whose distribution is of the exponential type, such as normal, gamma, or exponential. - no shape parameter

a) Common reliability laws

Distribution	Comments
Birnbaum-Saunders	<ul style="list-style-type: none"> - probabilistic model based on the restrictive assumption that fatigue crack growth is independent of crack length.
'Provan'	<ul style="list-style-type: none"> - derived from a probabilistic micromechanics model of fatigue crack propagation - more applicable for components - no shape parameter

b) Fatigue crack growth reliability laws.

Table 2.1 Main characteristics of the reliability laws.

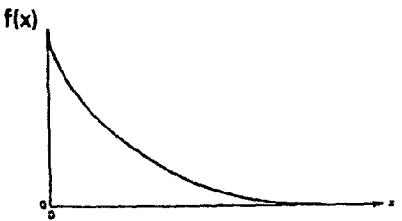
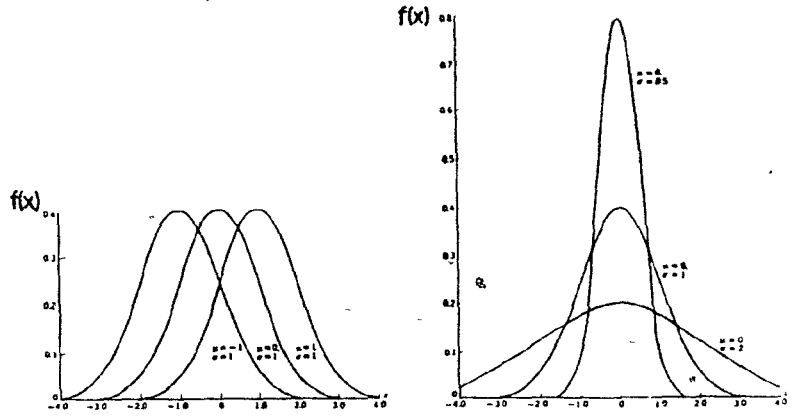
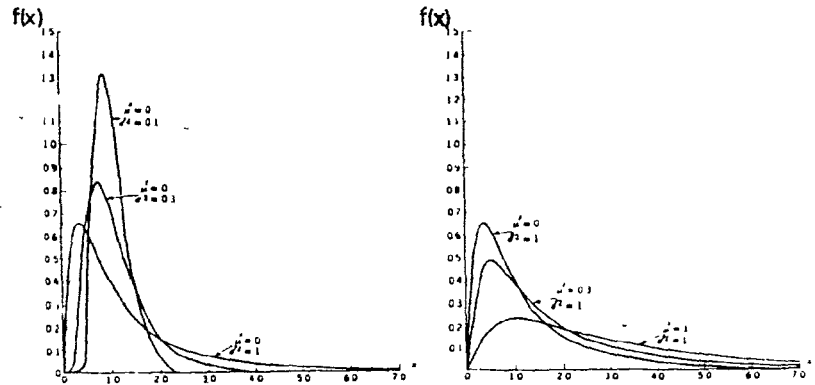
Distribution Name	Plots	Probability Density Function
Exponential		$f(x) = \frac{1}{\delta} \exp \left(\frac{-x}{\delta} \right)$
Normal		$f(x) = \frac{1}{\sigma\sqrt{2\pi}} \exp \left[-\frac{1}{2} \left(\frac{x-\mu}{\sigma} \right)^2 \right]$
Log-Normal		$f(x) = \frac{1}{\sigma'x\sqrt{2\pi}} \exp \left[-\frac{1}{2} \left(\frac{\ln x - \mu'}{\sigma'} \right)^2 \right]$

Table 2.2a) Exponential, normal and log normal probability density functions.

Distribution Name	Plots	Probability Density Function
Gamma		$f(x) = \frac{\alpha^\eta x^{\eta-1}}{\Gamma(\eta)} e^{-\alpha x}$
Weibull		$f(x) = \frac{\beta x^{\beta-1}}{\theta^\beta} \exp \left[-\left(\frac{x}{\theta}\right)^\beta \right]$
Gumbel		<p>Largest:</p> $f(x) = \frac{1}{\delta} \left[-\frac{1}{\delta} (x-\alpha) - \exp \left(\frac{x-\alpha}{\delta} \right) \right]$ <p>Smallest:</p> $f(x) = \frac{1}{\delta} \exp \left[\frac{1}{\delta} (x-\alpha) - \exp \left(\frac{x-\alpha}{\delta} \right) \right]$

Table 2.2b) Gamma, Weibull and Gumbel probability density functions.

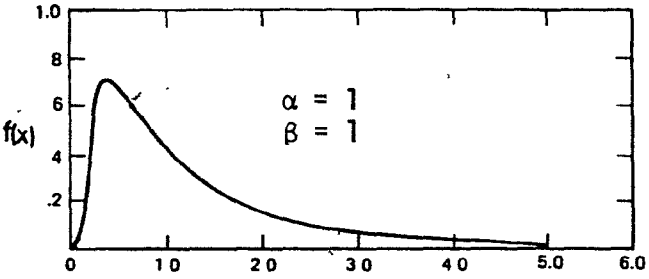
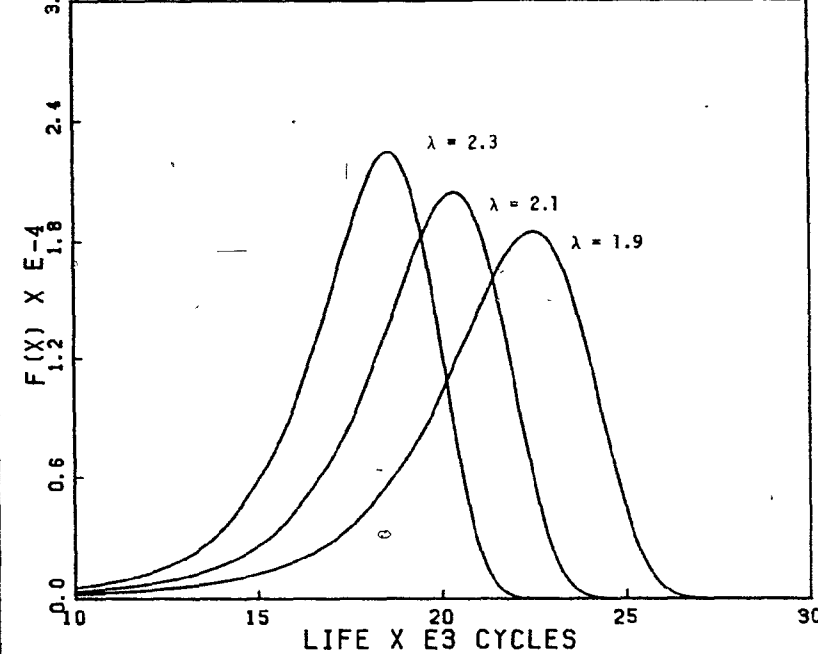
Distribution Name	Plots	Probability Density Function
Birnbaum-Saunders	 <p>$\alpha = 1$ $\beta = 1$</p>	$f(x) = \text{Eq. (2.34)}$
Provan	 <p>$\lambda = 2.3$ $\lambda = 2.1$ $\lambda = 1.9$</p>	$f(x) = \text{Eq. (2.41)}$

Table 2.2c) Birnbaum-Saunders and Provan probability density functions.

Distribution	Parameters	Cumulative Distribution Function	Mean	Variance
Exponential	$\delta > 0$	$F(x) = 1 - e^{-x/\delta}$	δ	δ^2
Normal	$-\infty < \mu < \infty$ $\sigma > 0$	$F(x) = \frac{1}{2} \operatorname{erfc}\left[\frac{-1}{\sqrt{2}} \left(\frac{x-\mu}{\sigma}\right)\right]$	μ	σ
Log Normal	$-\infty < \mu' < \infty$ $\sigma' > 0$	$F(x) = \frac{1}{2} \operatorname{erfc}\left[\frac{-1}{\sqrt{2}} \left(\frac{\ln x - \mu'}{\sigma'}\right)\right]$	$e^{\mu' + \sigma'^2/2}$	$e^{2\mu' + \sigma'^2} \times (e^{\sigma'^2} - 1)$
Gamma	$\alpha > 0$ $\eta > 0$	$F(x) = I\left[\frac{\alpha x}{\eta}, (\eta-1)\right]$	$\frac{\eta}{\alpha}$	$\frac{\eta}{\alpha^2}$
Weibull (2 parameters)	$\theta > 0$ $\beta > 0$	$F(x) = 1 - \exp\left[-\left(\frac{x}{\theta}\right)^\beta\right]$	$\theta \Gamma\left(\frac{1}{\beta} + 1\right)$	$\theta^2 \left\{ \Gamma\left(\frac{2}{\beta} + 1\right) - \left[\Gamma\left(\frac{1}{\beta} + 1\right)\right]^2 \right\}$
Weibull (3 parameters)	$\theta > 0, \theta_0 > 0$ $\beta > 0$	$F(x) = 1 - \exp\left[-\left(\frac{x-\theta_0}{\theta-\theta_0}\right)^\beta\right]$	$\theta_0 + (\theta - \theta_0) \Gamma\left(\frac{1}{\beta} + 1\right)$	$(\theta - \theta_0)^2 \left\{ \Gamma\left(\frac{2}{\beta} + 1\right) - \left[\Gamma\left(\frac{1}{\beta} + 1\right)\right]^2 \right\}$
Gumbel (largest value)	$-\infty < \alpha < \infty$ $\delta > 0$	$F(x) = \exp\{-\exp[-(\frac{x-\alpha}{\delta})]\}$	$\alpha + 0.5776\delta$	$1.645 \delta^2$
Gumbel (smallest value)	$-\infty < \alpha < \infty$ $\delta > 0$	$F(x) = 1 - \exp[-\exp(\frac{x-\alpha}{\delta})]$	$\alpha - 0.5776\delta$	"

a) Common reliability laws

Distribution	Parameters	Cumulative Distribution Function	Mean	Variance
Birnbaum-Saunders	$\alpha > 0$ $\beta > 0$	$F(x) = \frac{1}{2} \operatorname{erfc}\left(\frac{-1}{\alpha\sqrt{2}} \left[\left(\frac{x}{\beta}\right)^{1/2} - \left(\frac{x}{\beta}\right)^{-1/2}\right]\right)$	$\beta(1 + \frac{\alpha^2}{2})$	$(\alpha\beta)^2(1 + \frac{5\alpha^2}{4})$
'Provan'	$\lambda > 0$ $Vac > 0$	$F(x) = \frac{1}{2} \left\{ \operatorname{erf}\left(\frac{\mu_{a_0} e^{\lambda x} - \mu_{a_f}}{\sqrt{2} Vac}\right) + \operatorname{erf}\left(\frac{\mu_{a_f}}{\sqrt{2} Vac}\right) \right\}$	known complex expression	known complex expression

b) Fatigue crack growth reliability laws.

Table 2.3 Reliability laws and their basic statistics.

Specification	Designation: Certified Grade OFHC Copper corresponding to ASTM Specification B170, Grade 1 Grain Size (avg.): 0.025 mm Heat Treatment: Annealed
Average Mechanical Properties*	Yield Strength: 68.8 MPa Tensile Strength: 200.0 MPa Modulus of Elasticity: 117,169 MPa Elongation (50.8mm): 45% Shear Strength: 137.8 MPa Hardness: Rockwell F45

* Flat products, 6.35 mm thick.

Table 3.1 Specification and mechanical properties
of OFHC brand copper.

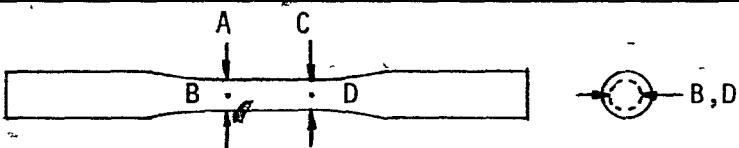
					
	A	B	C	D	Overall
Mean (mm)	9.40	9.41	9.41	9.40	9.40
Standard Deviation (mm)	0.026	0.022	0.027	0.026	0.025

Table 3.2 Statistics of the specimen test section measurements.

<u>FATIGUE SPECIMEN</u>	
Material	OFHC Brand Copper
Dimensions	see Fig. 3.1.
Stress Concentration Factor	unnotched
Preparation	rough turning on a conventional lathe, finish turning on N/C lathe
Thermal Treatment	stress relief annealing
Surface Treatment	hand polishing (average surface roughness: 0.5 μm)
Remarks	specimens stored in moisture-free containers before testing
<u>FATIGUE TESTS</u>	
Fatigue Testing Machine	100 kN MTS closed-loop electro hydraulic testing machine
Type of Test	strain-controlled axial
Test Frequency	1 Hz
Strain Amplitude	0.003
Strain Ratio (R)	-1
Strain Monitoring Device	2.5 cm MTS axial extensometer
Failure Criterion	complete fracture
Number of Specimens Tested	30

Table 4.1 Summary of the fatigue test conditions.

Specimen #	Life, N	Probability of Failure (Rank)
	Cycles	%
1	13622	3.8
2	14980	9.2
3	15926	14.6
4	17361	20.1
5	18013	25.5
6	18997	31.0
7	19120	36.4
8	19128	41.8
9	20271	47.3
10	20536	52.7
11	20616	58.2
12	21729	63.6
13	21740	69.0
14	22560	74.5
15	23241	80.0
16	23312	85.4
17	26150	90.8
18	27725	96.2

Table 4.2 Ranked fatigue data

Distribution	Parameters	Error = $\left(\frac{1}{18} \sum_{i=1}^{18} E_i^2 \right)^{1/2}$
Exponential	$\alpha = 16,060$ cycles $\delta = 4419$ "	0.222
Normal	$\mu = 20,280$ cycles $\sigma = 3,653$ "	0.029
Log Normal	$\mu' = 9.902$ $\sigma' = 0.184$	0.036
Gamma	$\alpha = 0.00152/\text{cycle}$ $\eta = 30.82$	0.032
Weibull (2 parameters)	$\theta = 21,770$ cycles $\beta = 6.269$	0.037
Gumbel (largest value)	$\alpha = 18,550$ cycles $\delta = 3,187$ "	0.049
Gumbel (smallest value)	$\alpha = 22,030$ cycles $\delta = 3,228$ "	0.053
Birnbaum-Saunders	$\beta = 19,960$ cycles $\alpha = 0.179$	0.036
Provan	$\lambda = 2.0E-4/\text{cycle}$ $Vac = 1.8E-5 \text{ m}^2$	0.048

Table 4.3 Curve-fit root mean square errors.

Distribution Name	Statistical Test	
	Komolgorov-Smirnov (Critical value: 0.309)*	Cramer-Von Mises (Critical Value: 0.461)*
Exponential	0.775 (rejected)	0.871 (rejected)
Normal	0.057 (accepted)	0.022 (accepted)
Log Normal	0.084 "	0.029 "
Gamma	0.073 "	0.024 "
Weibull (2 parameters)	0.073 "	0.032 "
Gumbel (largest value)	0.109 "	0.049 "
Gumbel (smallest value)	0.106 "	0.058 "
Birnbaum- Saunders	0.082 "	0.029 "
Provan	0.091 "	0.046 "

* for a sample size of 18 and a level of significance of 0.05

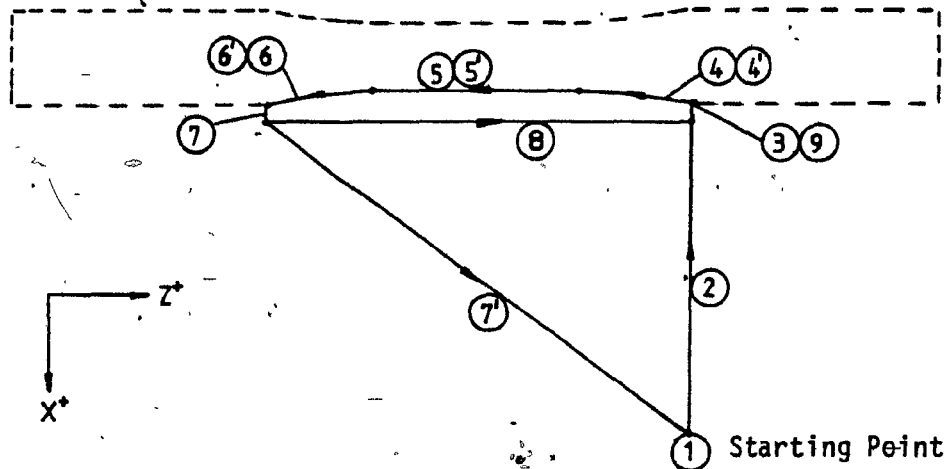
Table 4.4 Results of the statistical tests.

Material	O.F.H.C. Copper
Strain Amplitude	0.003
Cycles to failure	17,361
λ_{th}	0.12×10^{-3}
λ_{exp}	1.87×10^{-3}
λ_{emp}	0.20×10^{-3}

Table 4.5 Theoretical, experimental and empirical values for the crack growth transition intensity parameter of the "Provan law".

APPENDIX A

NUMERICALLY CONTROLLED MACHINING STEPS.



Step #	Description
N001	S08 1011
N002	X-17000 F100
N003	X-00400 F005
N004	X-00625 Z-06090 I29375 K-06090
N005	Z-11250
N006	X00625 Z-06090 I30000
N007	X01000 F100
N008	Z23430 F100
N009	X-01100 F004
N004	X-00625 Z-06090 I29375 K-06090
N005	Z-11250
N006	X00625 Z-06090 I30000
N007	X17500 Z23430 F100

APPENDIX B

STEP-BY-STEP TESTING PROCEDURE FOR THE FATIGUE EXPERIMENTS

Assuming that the static and dynamic (if necessary) calibrations and the preliminary adjustments have been performed for all electronic modules in accordance with the procedures described in the MTS owner's reference manuals, the test protocol reads as follows:

Step 1: Turn on the CONSOLE POWER.

Step 2: Select the 100% STROKE control mode and adjust SET POINT until the DC ERROR indicated on the controller METER is zero.

Step 3: Press INTERLOK RESET and RESET switches.

Step 4: Select a 1 Hz sinewave on the function generator and put it on REMOTE CONTROL MODE.

Step 5: Supply the power to the HPS unit and open the water circuit going through the heat exchanger.

Step 6: Press the HYDRAULIC PRESSURE switch twice and adjust the SET POINT to 500.

Step 7: Depress the PROGRAM AND RECORD switch and slowly set the SPAN 1 dial to 1. Let the system warm-up for about 30 minutes.

Step 8: Set back the SPAN 1 to zero and press again the PROGRAM AND RECORD switch.

Step 9: Press once the HYDRAULIC PRESSURE switch before pressing the HYDRAULIC OFF red button.

STEP 10: Select the 20% LOAD control mode and null the DC ERROR displayed on the front panel METER by turning the ZERO potentiometer of the

load d.c. conditioner. This zero can also be set from the readout of the data display module.

Step 11: Press the RESET switch and then the HYDRAULIC PRESSURE switch twice. If necessary, readjust the dual servovalve BALANCE (on the valve driver module) to stabilize actuator piston.

Step 12: Before fixing the extensometer on the specimen, stick two layers of adhesive copper tape on the specimen test section at the knife edge contact points.

Step 13: Set the hydraulic pressure to 6.9 MPa (1000 psi) using the main pressure control valve on the HPS unit (see Fig. 3.4).

Note: At this pressure, the gripping force was found sufficient to avoid specimen slippage while specimen crushing was minimized.

Step 14: Clamp the upper part (the one with the punched number at the top) of the specimen by turning the appropriate valve on the grip control unit.

Step 15: Connect the extensometer, remove its locking pin and adjust to zero the output of the strain d.c. conditioner by means of the ZERO potentiometer.

Step 16: Clamp the lower part of the specimen and progressively apply a 3kN tensile load on the specimen for alignment.

Step 17: Lock the grips and release the load.

Step 18: Rezero the strain d.c. conditioner output, if necessary, before pressing on the HYDRAULIC PRESSURE switch. Then, shut off the system.

Step 19: Select the 10% STRAIN control mode and press the RESET button before pressing the HYDRAULIC PRESSURE switch twice. Remove the load on the specimen, if any, by turning the ZERO dial of the strain d.c. conditioner.

Step 20: Reset both the ACTUAL COUNT and the TOTAL COUNT registers. Set the PRESET COUNT register to 3,000,000 and the counter input selector to OSCILLATORY.

Step 21: Press the PROGRAM AND RECORD switch and set gradually SPAN 1 to a $\pm 0.30\%$ strain which must be read on the data display module.

Step 22: Set STROKE LIMIT DETECTOR according to the PEAK TO PEAK readout of the data display unit then put in an INTERLOCK mode.

Step 23: Set the upper limit to 10 and the lower limit to 0.2 on the LOAD LIMIT detector and select the INTERLOCK mode.

Note: The load rectifier circuit (Fig. 3.8) has been previously connected to this limit detector.

Step 24: After specimen failure remove the extensometer (HPS unit being off). Then perform step 11 again for releasing the specimen. When manipulating the specimen, great caution must be taken to prevent any damage to the fatigue fracture surfaces.

Remark: The IND mode must be selected on all limit detectors before restarting the HPS unit.

Step 25: If another test is to be performed immediately, return to step 12 and carry on the procedure. If not, shut off the system and start from step 1 for the subsequent test.

APPENDIX C

COMPLEMENTARY INFORMATION

C.1 THE HAZARD-RATE-CONCEPT

The concept of hazard rate is often referred to in reliability in order to choose, among the possible distribution functions for a given problem, the more appropriate failure model, on the basis of physical considerations.

Let $F(t)$ be the cumulative distribution function of the time-to-failure random variable T , and let $f(t)$ be its probability density function. The probability of failure in a given time interval $[t_1, t_2]$ is then expressed as

$$\int_{t_1}^{t_2} f(t)dt = \int_{-\infty}^{t_2} f(t)dt - \int_{-\infty}^{t_1} f(t)dt = F(t_2) - F(t_1)$$

The rate at which failure occurs in the same time interval is called the failure rate during that interval and is specifically defined as the probability that a failure per unit time occurs in the interval, given that a failure has not occurred prior to t_1 , the beginning of the interval. Thus, the failure rate is written as:

$$\frac{F(t_2) - F(t_1)}{(t_2 - t_1)(1 - F(t_1))} \quad (C.1)$$

which is a function of time. Redefining the time interval as $[t, t + \Delta t]$, Equation (C.1) becomes:

$$\frac{F(t + \Delta t) - F(t)}{\Delta t [1 - F(t)]}$$

Hence, the hazard rate is defined as the limit of the failure rate as the time interval approaches zero. In other words, the hazard rate is the instantaneous failure rate and is expressed by:

$$h(t) = \lim_{\Delta t \rightarrow 0} \frac{F(t+\Delta t) - F(t)}{\Delta t [1 - F(t)]} = \frac{1}{1 - F(t)} \left[\frac{dF(t)}{dt} \right] \quad (C.2)$$

$$= \frac{f(t)}{1 - F(t)}$$

A classical hazard function is the so-called bathtub curve shown in Fig. C.1. In this curve appears the three major types of failures that generally assist the choices of $h(t)$. First, there is the burn-in period that represents the early failure often attributable to manufacturing defects. Subsequently, $h(t)$ remains approximately constant until time t_1 and corresponds to the "chance failure" that results from unpredictable conditions occurring during the operating time of the device. The third type, called the wear-out failure, is associated with a gradual material deterioration caused by an accumulation of shocks, fatigue, and so on.

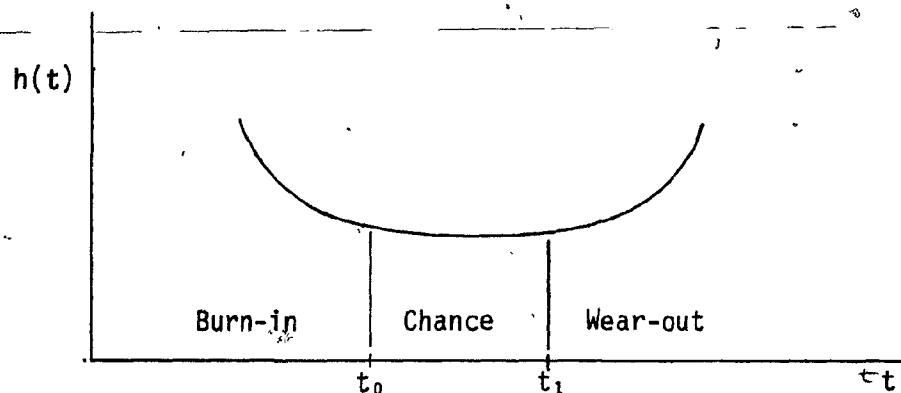


Fig. C.1 The bathtub curve.

C.2 THE CENTRAL LIMIT THEOREM

One of the most important results of mathematical statistics is the central limit theorem that provides the theoretical justification for the important role played by the normal distribution in statistics. This theorem states that the distribution of the mean of n independent observations from any distribution, or even from n different distributions, with finite mean and variance approaches a normal distribution as the number of observations n approaches infinity.

The central limit theorem is also applicable for relatively small samples as long as no single element or small group of elements has a dominant variance and the element distributions do not deviate too much from a normal distribution.

C.3 PARAMETER ESTIMATING METHODS FOR THE CDF

C.3.1 Method of Matching Moments

Let x be a random variable with a density function $f_x(x; \epsilon_1, \epsilon_2, \dots, \epsilon_k)$, where ϵ_i 's are the parameters to estimate. Next, let us define the t^{th} moment of f_x about zero as:

$$\mu_t' = \int_{-\infty}^{\infty} x^t f_x(x; \epsilon_1, \epsilon_2, \dots, \epsilon_k) dx \quad (C.3)$$

From this equation one can see that μ_t' is a function of the k parameter.

Now, if x_1, x_2, \dots, x_n represents a random sample of size n from f_x , the first k sample moments are defined as:

$$m_t' = \frac{1}{n} \sum_{i=1}^n x_i^t, \quad t = 1, 2, \dots, k \quad (C.4)$$

Hence, the moment estimators $\hat{\epsilon}_i$, $i = 1, \dots, k$ of the ϵ_i 's are obtained by solving the following equations for the ϵ_i 's:

$$\mu_t' = m_t' \quad t = 1, 2, \dots, k$$

C.3.2 Method of Maximum-Likelihood

The method of maximum-likelihood involves taking, as the estimate for each unknown parameter, the value that appears most probable on the basis of the given data. Thus, the likelihood function of random sample, x_1, x_2, \dots, x_n , drawn from a multiparameter density function $f_X(x; \gamma_1, \gamma_2, \dots, \gamma_k)$ is defined as the joint density of the n random variables, x_i 's, and is written as:

$$L = \prod_{i=1}^n f_{X_i}(x_i; \gamma_1, \gamma_2, \dots, \gamma_k) \quad (C.5)$$

Hence, the maximum-likelihood estimators of the γ_i 's, say $\hat{\gamma}_i = h_i(x_1, x_2, \dots, x_n)$, $i = 1, 2, \dots, k$, are the values of the γ_i 's that maximize $\log L$ and are obtained by solving:

$$\frac{\partial \log L}{\partial \gamma_i} = 0 \quad i = 1, 2, \dots, k$$

C.3.3 The Method of Least Squares

The method of least squares is used to determine the best fit of an assumed implicit function to the experimental data. This is done by minimizing the sum of the squares of the deviation in the y direction of the data points from the most probable curve. For the case where one desires to fit a straight line say $y = Ax + B$ to the data points (x_i, y_i) , the problem resumes to minimize:

$$E = \sum_{i=1}^n (y_i - Ax_i - B)^2, \quad (C.6)$$

by finding the appropriate values for A and B. These values are simply obtained by deriving (C.6) with respect to A and B and by setting the result equal to zero, namely:

$$\frac{\partial E}{\partial A} = -2 \sum_{i=1}^n (y_i - Ax_i - B)x_i, \quad (C.7)$$

$$\frac{\partial E}{\partial B} = -2 \sum_{i=1}^n (y_i - Ax_i - B), \quad (C.8)$$

Solving the above equations for A and B, one finally obtains:

$$A = \frac{n \sum(xy) - (\sum x)(\sum y)}{n \sum(x^2) - (\sum x)^2}, \quad (C.9)$$

$$B = \frac{\sum y \sum(x^2) - \sum x \sum(xy)}{n \sum(x^2) - (\sum x)^2}, \quad (C.10)$$

where $\sum x = \sum_{i=1}^n x_i$, $\sum y = \sum_{i=1}^n y_i$, and $\sum xy = \sum_{i=1}^n x_i y_i$.

APPENDIX D

DERIVATION OF THE "PROVAN" CDF

By definition, the cumulative distribution function is expressed as

$$CDF(x) = \int_{-\infty}^x p.d.f.(\alpha) d\alpha$$

Hence, from Eq. (2.41) we have:

$$\begin{aligned} P_{NP}(j) &= \int_{-\infty}^j p_{NP}(i) di \\ &= \frac{\mu_{a_0}}{\sqrt{2\pi}V_{ac}} \int_{-\infty}^j \exp\left\{\lambda i - \frac{(\mu_{a_0} \exp[\lambda i] - \mu_{af})^2}{2V_{ac}}\right\} di. \end{aligned} \quad (D.1)$$

Now, the change of variable:

$$z^2 = \frac{(\mu_{a_0} \exp[\lambda i] - \mu_{af})^2}{2V_{ac}}, \quad (D.2)$$

yields: $\sqrt{2V_{ac}} z = \mu_{a_0} \exp[\lambda i] - \mu_{af}$, and deriving we get:

$$\frac{\sqrt{2V_{ac}}}{\mu_{a_0} \lambda} dz = \exp[\lambda i] di \quad (D.3)$$

Looking at the limits of integration, we have from (D.2) that:

$$\begin{aligned} \text{when } i = -\infty \quad z_{-\infty}^2 &= \left(\frac{-\mu_{af}}{\sqrt{2V_{ac}}} \right)^2, \\ \therefore z_{-\infty} &= \frac{-\mu_{af}}{\sqrt{2V_{ac}}} \end{aligned} \quad (D.4)$$

and when $i = j$

$$z_j = \frac{\mu_{a_0} \exp[\lambda_j] - \mu_{af}}{\sqrt{2V_{ac}}} \quad (D.5)$$

Substituting equations (D.3), (D.4) and (D.5) into (D.1), we obtain:

$$\begin{aligned} P_{NP}(j) &= \frac{1}{\sqrt{\pi}} \int_{z_{-\infty}}^{z_j} e^{-z^2} dz, \\ &= \frac{1}{2} \left[\frac{2}{\sqrt{\pi}} \int_0^{z_j} e^{-z^2} dz - \frac{2}{\sqrt{\pi}} \int_0^{z_{-\infty}} e^{-z^2} dz \right] \end{aligned} \quad (D.6)$$

But, knowing that

$$\frac{2}{\sqrt{\pi}} \int_0^x e^{-z^2} dz$$

is by definition the error function, (D.6) becomes:

$$P_{NP}(j) = \frac{1}{2} [\text{erf}(z_j) - \text{erf}(z_{-\infty})] \quad (D.7)$$

Finally, substituting back equation (D.5) for z we get:

$$P_{NP(j)} = \frac{1}{2} \left\{ \operatorname{erf} \left(\frac{\mu_{a_0} \exp[\lambda_j] - \mu_{a_f}}{\sqrt{2V_{ac}}} \right) + \operatorname{erf} \left(\frac{\mu_{a_f}}{\sqrt{2V_{ac}}} \right) \right\} \quad (D.8)$$

which recovers equation (2.42).

APPENDIX E

CURVE FITTING PROGRAMS

E.1 OPTIMIZING PROGRAM FOR THE "PROVAN LAW"

```

C
C
C
*****
*                               PROV AN'S CDF                               *
*****
REAL *4 LAMBDA,MUAF,MUAO
DIMENSION PP(18),X(18),ERR(18),Z(18)
DATA X/13622.,14980.,15926.,17361.,18013.,18997.,
*19120.,19128.,20271.,20536.,20613.,21729.,21740.,
*22560.,23241.,23312.,26150.,27725.,P/.038,.092,
*.146,.201,.255,.31,.364,.418,.473,.527,.582,
*.636,.69,.745,.8,.854,.908,.962/
WRITE(6,100)
MUAF=9.53E-3
MUAO=1.55E-4
VAC=2.1E-5
LAMBDA=1.7E-4
DO 25 K=1,6
  LAMBDA=LAMBDA+.1E-4
DO 20 I=1,5
  VAC=VAC-.1E-5
DO 15 I=1,18
  Z(I)=(MUAF-MUAO*EXP(LAMBDA*X(I)))/SQRT(2*VAC)
15 ERR(I)=ABS(1.+ERF(-Z(I)/SQRT(2.)))/2)
  E=RMS(ERR)
WRITE(6,110) LAMBDA,VAC,E
WRITE(6,105) ERR
20 CONTINUE
25 CONTINUE
100 FORMAT(///' PROV AN CDF'///)
105 FORMAT(1X,E15.6/)
110 FORMAT(1X,3E15.6/)
  STOP
  ENO

C
FUNCTION RMS(ERR)
DIMENSION ERR(18)
SUM=0.
DO 5 I=1,18
5 SUM=SUM+ERR(I)**2
RMS=SQRT(SUM/18)
RETURN
END

```

E.2 ESTIMATING PROGRAM FOR THE OTHER INVESTIGATED LAWS

```

*****
*
*           BEST CDF THROUGH A SET OF LIFE DATA
*           *****
*
*****

```

```

IMPLICIT REAL*8(A-H,M-Z)
REAL *4 ZET,T,W,PROB
DIMENSION N(18),P(18),ERR(18),Y(18),X(18)
DATA N/13622.00,14980.00,15926.00,17361.00,18013.00,18997.00,
*19120.00,19128.00,20271.00,20536.00,20613.00,21729.00,21740.00,
*22560.00,23241.00,23312.00,26150.00,27725.00/,P/.03800,.09200,
*.14600,.20100,.25500,.3100,.36400,.41800,.47300,.52700,.58200,
*.63600,.69000,.74500,.80000,.85400,.90800,.96200/

```

2-PARAMETER WEIBULL

```

DO 5 I=1,18
X(I)= DLOG(N(I))
5 Y(I)=DLOG(DLOG(1/(1.00-P(I))))
CALL SQFIT(X,Y,SLOPE,C)
NA=DEXP(-C/SLOPE)
DO 10 I=1,18
10 ERR(I)=DABS(1.00-DEXP(-(N(I)/NA)**SLOPE)-P(I))
E=RMS(ERR)
WRITE(6,100)
WRITE(6,105) SLOPE,NA,E
WRITE(6,106)ERR

```

NORMAL

```

MEAN=0.00
DO 11 I=1,18
11 MEAN=(MEAN*(I-1)+N(I))/I
SUM5=0.00
DO 15 I=1,18
15 SUM5=SUM5+(N(I)-MEAN)**2
SIG=DSQRT(SUM5/17)
DO 20 I=1,18
20 ERR(I)= CABS( DERFC( (MEAN-N(I))/SIG/DSQRT(2.00) )/2-P(I) )
E=RMS(ERR)
WRITE(6,110)
WRITE(6,105) MEAN,SIG,E
WRITE(6,106)ERR

```

LOG-NORMAL

```

MEANLN=0.00
DO 29 I=1,18
29 MEANLN=(MEANLN*(I-1)+DLOG(N(I)))/I
SUM6=0.00
DO 30 I=1,18
30 SUM6=SUM6+(DLOG(N(I))-MEANLN)**2
SIGLN=DSQRT(SUM6/17)
DO 35 I=1,18
35 ERR(I)=DABS( DERFC( (MEANLN-DLOG(N(I)))/SIGLN/DSQRT(2.00) )/2-P(I) )
E=RMS(ERR)
WRITE(6,115)
WRITE(6,105) MEANLN,SIGLN,E
WRITE(6,106)ERR

```

C

EXPONENTIAL

```
DO 40 I=1,18
40 Y(I)=DLOG(1-P(I))
CALL SQFIT(N,Y,SLOPE,C)
DO 45 I=1,18
45 ERR(I)=DABS(1.D0-DEXP(SLOPE*N(I)+C)-P(I))
E=RMS(ERR)
WRITE(6,120)
WRITE(6,105) SLOPE,C,E
WRITE(6,106)ERR
```

C
C
C

GAMMA

```
ELAM=MEAN/SIG**2
ZETA=ELAM*MEAN
DO 50 I=1,18
ZET=ZETA
T=ELAM*N(I)
CALL MDGAM(T,ZET,PROB,IER)
W=P(I)
50 ERR(I)=ABS(PROB-W)
E=RMS(ERR)
WRITE(6,125)
WRITE(6,105) ELAM,ZETA,E
WRITE(6,106) ERR
```

C
C
C

GUMBEL(SMALLEST)

```
DO 55 I=1,18
55 Y(I)=DLOG(DLOG(1/(1.D0-P(I))))
CALL SQFIT(N,Y,SLOPE,C)
DO 60 I=1,18
60 ERR(I)=DABS(P(I)-1.D0+DEXP(-DEXP(N(I)*SLOPE+C)))
E=RMS(ERR)
WRITE(6,130)
WRITE(6,105)SLOPE,C,E
WRITE(6,106)ERR
```

C
C
C

GUMBEL(LARGEST)

```
DO 65 I=1,18
65 Y(I)=DLOG(DLOG(1/P(I)))
CALL SQFIT(N,Y,SLOPE,C)
DO 70 I=1,18
70 ERR(I)=DABS(P(I)-DEXP(-DEXP(SLOPE*N(I)+C)))
E=RMS(ERR)
WRITE(6,135)
WRITE(6,105)SLOPE,C,E
WRITE(6,106)ERR
```

C
C
C

BIRNBAUM-SAUNDERS

```
S=0.D0
RR=0.D0
DO 75 I=1,18
S=(S*(I-1)+N(I))/I
75 RR=(RR*(I-1)+1/N(I))/I
R=1/RR
BETA=DSQRT(S*R)
ALPHA=DSQRT(S/BETA+BETA/R-2.D0)
DO 80 I=1,18
W=DSQRT(N(I)/BETA)
Z=1/ALPHA*(W-1/W)
80 ERR(I)=DABS(DEFRC(-Z/DSQRT(2.D0))/2-P(I))
E=RMS(ERR)
WRITE(6,140)
WRITE(6,105)ALPHA,BETA,E
WRITE(6,106)ERR
```

```
100 FORMAT(////' 2-PARAMETER WEIBULL'////)
105 FORMAT(1X,3D20.12//)
106 FORMAT(1X,D20.12//)
110 FORMAT(////' NORMAL'////)
115 FORMAT(////' LOG-NORMAL'////)
120 FORMAT(////' EXPONENTIAL'////)
125 FORMAT(////' GAMMA'////)
130 FORMAT(////' GUMBEL(SMALLEST)'////)
135 FORMAT(////' GUMBEL(LARGEST)'////)
140 FORMAT(////' BIRNBAUM-SAUNDERS'////)
STOP
END
```

C

```
FUNCTION RMS(ERR)
IMPLICIT REAL*8(A-H,O-Z)
DIMENSION ERR(18)
SUM=0.00
DO 5 I=1,18
5 SUM=SUM+ERR(I)**2
RMS=DSQRT(SUM/18)
RETURN
END
```

C

```
SUBROUTINE SQFIT(X,Y,SLOPE,C)
IMPLICIT REAL*8(A-H,O-Z)
DIMENSION X(18),Y(18)
SUM1=0.00
SUM2=0.00
SUM3=0.00
SUM4=0.00
DO 5 I=1,18
SUM1=SUM1+Y(I)
SUM2=SUM2+X(I)
SUM3=SUM3+Y(I)*X(I)
5 SUM4=SUM4+X(I)**2
SLOPE=(18.00*SUM3-SUM2*SUM1)/(18.00*SUM4-SUM2**2)
C=(SUM1*SUM4-SUM2*SUM3)/(18.00*SUM4-SUM2**2)
RETURN
END
```


APPENDIX F

PLOTTING PROGRAM

```
EXTERNAL EXPO,NORM,LOGN,GAM,GUMS,GUML,PROV,WEIB,BS
DIMENSION Y(20),X(20),XX(20),YY(20)
DATA X/13622.,14980.,15926.,17361.,18013.,18997.,19120.,
*19128.,20271.,20536.,20616.,21729.,21740.,22560.,23241.,
*23312.,26150.,27725.,0.,0./,Y/.038,.092,.146,.201,.255,.31,
*.364,.418,.473,.527,.582,.536,.69,.745,.8,.854,.908,.962,
*0.,0./
```

```
CALL PLOTEN
CALL PLOT(1.0,2.,-3)
CALL AXS(0.0,0.0,16H LIFE X E3 CYCLES,-16,-6.,0.0,10.,5.,
*-1.0,.1.5)
CALL AXS(0.0,0.,3H CDF,3,-5.,90.,0.,0.2,1.0,.1.0)
CALL AXS(6.,0.,11H RELIABILITY,-11,-5.,90.,1.,-2.1,0.,1.)
CALL PLCT(0.,5.,3)
CALL PLOT(6.,5.,2)
DO 5 I=1,18
XX(I)=(X(I)-1.E4)/5000.*1.5-.045
YY(I)=Y(I)*5-.045
CALL SYMBCL(XX(I),YY(I),.09,1.0,-1)
```

5 CONTINUE

```
CALL FNPLT(1.82,6.,1,EXPO)
CALL SYMBOL(.5,5.5,.15,11H EXPONENTIAL,0.,11)
CALL SYMBOL(.5,4.2,.12,21H DELTA= 4.419E3 CYCLES,0.,21)
CALL SYMBOL(.5,4.5,.12,21H ALPHA= 1.606E4 CYCLES,0.,21)
CALL FNPLT(0.,6.,1,NORM)
CALL SYMBOL(.5,5.5,.15,6H NORMAL,0.,6)
CALL SYMBCL(.5,4.5,.12,18H MU= 2.028E4 CYCLES,0.,18)
CALL SYMBOL(.5,4.2,.12,21H SIGMA= 3.653E3 CYCLES,0.,21)
CALL FNPLT(0.,6.,1,LOGN)
CALL SYMBOL(.5,5.5,.15,10H LOG-NORMAL,0.,10)
CALL SYMBOL(.5,4.5,.12,10H MU= 9.902,0.,10)
CALL SYMBOL(.5,4.2,.12,16H SIGMA= 1.839E-1.0.,16)
CALL FNPLT(0.,6.,1,GAM)
CALL SYMBOL(.5,5.5,.15,5H GAMMA,0.,5)
CALL SYMBOL(.5,4.5,.12,22H ALPHA= 1.520E-3/CYCLES,0.,22)
CALL SYMBOL(.5,4.2,.12,12H DELTA= 3.082E1,0.,12)
CALL FNPLT(0.,6.,1,GUMS)
CALL SYMBOL(.5,5.5,.15,16H GUMBEL(SMALLEST),0.,16)
CALL SYMBOL(.5,4.2,.12,21H DELTA= 3.228E3 CYCLES,0.,21)
CALL SYMBOL(.5,4.5,.12,21H ALPHA= 2.203E4 CYCLES,0.,21)
CALL FNPLT(0.,6.,1,GUML)
CALL SYMBOL(.5,5.5,.15,15H GUMBEL(LARGEST),0.,15)
CALL SYMBOL(.5,4.2,.12,21H DELTA= 3.187E3 CYCLES,0.,21)
CALL SYMBOL(.5,4.5,.12,21H ALPHA= 1.805E4 CYCLES,0.,21)
CALL FNPLT(0.,6.,1,PROV)
CALL SYMBOL(.5,5.5,.15,6H PROVAN,0.,6)
CALL SYMBOL(.5,4.5,.12,21H LAMBDA= 2.0E-4/CYCLES,0.,21)
CALL SYMBOL(.5,4.2,.12,13H VAC= 1.8E-5 M,0.,13)
CALL FNPLT(0.,6.,1,WEIB)
CALL SYMBOL(.5,5.5,.15,7H WEIBULL,0.,7)
CALL SYMBOL(.5,4.5,.12,21H THETA= 2.177E4 CYCLES,0.,21)
CALL SYMBOL(.5,4.2,.12,11H BETA= 6.269,0.,11)
CALL FNPLT(0.,6.,1,BS)
CALL SYMBOL(.5,5.5,.15,17H BIRNBAUM-SAUNDERS,0.,17)
CALL SYMBOL(.5,4.5,.12,15H ALPHA= 1.794E-1.0.,15)
CALL SYMBOL(.5,4.2,.12,20H BETA= 1.996E4 CYCLES,0.,20)
CALL ENDPLOT
STOP
END
```

FUNCTION EXPO(X)

SCA=X*5000./1.5+1.E4
A=-.226314E-3
B=.363521E1
EXPO=(1-EXP(A*SCA+B))*5
RETURN
END

FUNCTION NORM(X)

REAL *4 MEAN

SCA=X*5000./1.5+1.E4
MEAN=.202791E5
SIG=.365261E4
NORM=ERFC((MEAN-SCA)/SIG/SQRT(2.))/2*5
RETURN
END

FUNCTION LOGN(X)

REAL *4 MEANLN

SCA=X*5000./1.5+1.E4
MEANLN=.990165E1
SIGLN=.183944
LOGN=ERFC((MEANLN-ALOG(SCA))/SIGLN/SQRT(2.))/2*5
RETURN
END

FUNCTION GAM(X)

SCA=X*5000./1.5+1.E4
ETA=.308242E2
ALPHA=.151999E-2
T=ALPHA*SCA
CALL MDGAM(T,ETA,PROB,IER)
GAM=PROB*5
RETURN
END

FUNCTION WEIB(X)

SCA=X*5000./1.5+1.E4
NA=.217661E5
SLOPE=.62693E1
WEIB=(1.-EXP(-(SCA/NA)**SLOPE))*5
RETURN
END

FUNCTION GUMS(X)

SCA=X*5000./1.5+1.E4
A=.309783E-3
B=-.682415E1
GUMS=(1.-EXP(-EXP(A*SCA+B)))*5
RETURN
END

C FUNCTION GUML(X)

SCA=X*5000./1.5+1.E4
A=-.313783E-3
B=.582075E1
GUML=EXP(-EXP(A*SCA+B))*5
RETURN
END

C FUNCTION PROV(X)
C REAL *4 MUAF,MUAO,LAMBDA

SCA=X*5000./1.5+1.E4
LAMBDA=.20E-3
VAC=.18E-4
MUAF=.953E-2
MUAO=.155E-3
Z=(MUAF-MUAO*EXP(LAMBDA*SCA))/SQRT(2*VAC)
PROV=(1.+ERF(-Z/SQRT(2.)))/2*5
RETURN
END

C FUNCTION BS(X)
C

SCA=X*5000./1.5+1.E4
ALPHA=.179406
BETA=.199579E5
W=SQRT(SCA/BETA)
Z=1/ALPHA*(W-1/W)
BS=ERFC(-Z/SQRT(2.))/2*5
RETURN
END